HYDROTHERMAL PREPARATION OF SINGLE CRYSTALLINE CeO_2 NANOPARTICLES AND THE INFLUENCE OF ALKALI HYDROXIDES ON THEIR STRUCTURE AND OPTICAL BEHAVIOR

A Thesis Submitted to
the Graduate School of Engineering and Science of
İzmir Institute of Technology
in Partial Fulfillment of the Requirements for the Degree of

MASTER OF SCIENCE

in Chemistry

by
Özlem KEPENEKCİ

June 2009
İZMİR

We approve the thesis of **Özlem KEPENEKCİ**

Assoc.Prof.Dr. Mehtap EMİRDAĞ EANES
Supervisor

Assoc.Prof.Dr. Mustafa Muammer DEMİR
Co-Supervisor

Prof.Dr. Serdar ÖZÇELİK
Committee Member

Assoc.Prof.Dr. Sedat AKKURT
Committee Member

Asst.Prof.Dr. Funda DEMİRHAN
Committee Member

19 June 2009

Date

Prof.Dr. Levent ARTOK
Head of the Chemistry Department

Prof.Dr. Hasan BÖKE
Dean of the Graduate School of
Engineering and Sciences

ACKNOWLEDGEMENTS

I will first and foremost like to thank my great supervisor Assoc. Prof. Mehtap EMİRDAG EANES who has supported me throughout my thesis with her endless patience. Whenever I had a problem, she always gave me her valuable advices. One simply could not wish for a better or friendlier supervisor.

Also, I would like to appreciate deeply my co-supervisor Assoc. Prof. Mustafa M. DEMİR for his kind support, valuable comments and understanding.

Next, I want to thank Dr. Ingo LIEBERWIRTH from Max-Planck Institute for Transmission Electron Microscope images and Center of Materials Research (IYTE MAM) for Scanning Electron Microscope and X-ray Diffraction analyses.

Additionally, I would like to thank my dearest friend Sumru ÖZÇİFTÇİ for her encouragement and never ending friendship. Whatever obstacles I come across, she always find a solution. I owe her so much.

Special thanks to all my friends in IZTECH especially Banu ÖNEN, Nesrin HORZUM, Pınar KASAPLAR and Seda ÖZDEMİR for their moral support.

Thanks to Özay GÖĞEBAKAN for believing me in every moment with her good thoughts.

Finally, my deepest gratitude goes to my family, my father Halil and my mother Lale, for their endless love, understanding and encouragement throughout my entire life. It would not be possible to complete this thesis without their support.

ABSTRACT

HYDROTHERMAL PREPARATION OF SINGLE CRYSTALLINE CeO_2 NANOPARTICLES AND THE INFLUENCE OF ALKALI HYDROXIDES ON THEIR STRUCTURE AND OPTICAL BEHAVIOR

Single crystalline cerium oxide nanoparticles were synthesized via hydrothermal method by mixing aqueous solution of cerium nitrate [$Ce(NO_3)_3.6H_2O$] with an alkali base. Several characterization methods were used to identify morphology and crystalline nature such as X-ray Diffraction, Scanning and Transmission Electron Microscopes.

This study is divided into three parts. In the first part, some controlling parameters like, that were affecting size and shape of CeO_2 nanoparticles, were studied. It was found that size of CeO_2 nanoparticles increased when increasing both reaction time and temperature. Alkali base concentration promoted the particle growth. Also, particle morphology was more uniform rather than aggregated in presence of higher concentrated alkali base. When the alkali base type was changed, the use of NaOH produced larger cubic nanocrystals of CeO_2 than KOH and LiOH.

Second part is related to determine the optical properties of CeO_2 nanoparticles. Based on the UV-Vis and Fluorescence Spectroscopy results, size, bandgap and defect level of CeO_2 nanoparticles can be easily determined. Nanoparticles in presence of NaOH alkali base were found to produce less defective CeO_2 nanoparticles as compared to KOH and LiOH.

The last part of this work is to evaluate the shape effect on morphology, size and optical properties of CeO_2 nanoparticles. Rod crystals of CeO_2 were produced when the hydrothermal synthesis temperature was low (120°C) or when the reaction time was short (1 hour). When the synthesis temperature was higher than 160°C well defined cubic crystals of CeO_2 started to form.

ÖZET

TEK KRİSTAL CeO_2 NANOPARÇACIKLARININ HİDROTERMAL YÖNTEMLE HAZIRLANMASI VE ALKALİ HİDROKSİTLERİN YAPI VE OPTİK ÖZELLİKLER ÜZERİNDEKİ ETKİSİ

Tek kristal seryum oksit nanoparçacıkları, seryum nitrat [$Ce(NO_3)_3.6H_2O$] ve alkali baz sulu çözeltisinin karıştırılmasından sonra hidrotermal metotla sentezlenmiştir. Morfoloji ve kristallik özelliği çeşitli karakterizasyon yöntemleri kullanılarak belirlenmiştir. Bu yöntemler X-ray kırınımı, Taramalı ve Geçirimli elektron mikroskoptur.

Bu tez çalışması üç parçaya ayrılmıştır. Çalışmanın birinci bölümünde, reaksiyona etki eden bazı etmenler üzerinde durulmuş ve bu etmenlerin nanoparçacıkların büyüklüğü ve şekli üzerindeki etkisine bakılmıştır. Reaksiyon süresi ve sıcaklığı arttırıldığında CeO_2 nanoparçacıklarının büyüklüğünde bir artış gözlemlenmiştir. Ayrıca bu etki alkali baz konsantrasyonunun artışında da görülmüştür. Konsantrasyonu yüksek alkali bazlarda morfoloji topaklanma yerine daha homojen dağılım göstermektedir. Alkali baz tipi değiştirildiğinde ise NaOH kullanımıyla oluşan kübik CeO_2 nanokristallerin KOH ve LiOH kullanımına göre daha büyük olduğu saptanmıştır.

İkinci bölüm seryum oksit nanoparçacıklarının optik özelliklerini araştırmaya yöneliktir. UV-Görünür ve Floresans Spektroskopi sonuçlarına göre seryum oksit nanoparçacıklarının bant aralığı, parçacık boyutu ve kristal kusurları kolayca incelenebilir. Buna göre, NaOH ile hazırlanan nanoparçacıklarında KOH ve LiOH bazlarına göre daha az kristal kusuru bulunmuştur. Ayrıca, yüksek sıcaklıklarda ve reaksiyon zamanlarında kristal kusurlarında azalma gözlemlenmiştir.

Son bölümde seryum oksit nanoparçacıklarının şekil farklılıkları morfoloji, parçacık boyutu ve optik özelliklerine etkisi incelenmiştir. Hidrotermal sentez sıcaklığı düşükken (120°C) veya reaksiyon süresi kısayken (1 saat) iğne şeklinde nanoparçacıkları oluşurken. 160°C'den sonra sıcaklık artışıyla kübik nanoparçacıklar oluşmuştur.

Dedicated to;

the memory of my grandfather

and

my lovely family for being with me in all my life…

TABLE OF CONTENTS

LIST OF FIGURES

LIST OF TABLES

Table **Page**

CHAPTER 1

INTRODUCTION

Nanotechnology is a field of science that involves the combination of chemistry, biology, physics and engineering subjects. It deals with small-sized materials in the nanometer (nm) scale ranging from 100 nm and down to a few nanometers. The prefix 'nano' is derived from the Greek word of 'nanos' meaning 'dwarf' and one nanometer is equal to one billionth of a meter (10^{-9} m). As an illustration, one carbon atom is 0.16 nm in diameter and the size of human hair is approximately 50 000 nm wide.

There are a lot of different definitions about what exactly nanotechnology is. In general it is a technology of fabrication, characterization, design and application of structures, devices and systems by controlling shape and size at nanometer scale (The Royal Society & The Royal Academy of Engineering 2004). Also, it has been defined as structures and components of materials or systems show novel and significantly improved physical, chemical and biological properties, phenomena and processes due to their nanoscale size (National Nanotechnology Initiative 2000).

In order to understand the concept of physical properties and phenomena of nanostructured materials, the fabrication and characterization of nanomaterials are the most important building blocks of nanotechnology. Nanostructured materials has at least one dimension in nanometer scale and include nanoparticles, nanorods, nanofibers, thin films, nanowires and bulk materials that mean very small particles with larger sizes than typical molecules. Nanoparticles have a characteristic dimension of the particles which is mostly less than a couple of hundred nanometers. Fabrication of nanoparticles has become challenging since a small size is not the only requirement. For better fabrication and using in many applications, resulting nanoparticles have the following characteristics (Cao 2004);

a. identical shape and morphology
b. identical crystal structure
c. individually dispersed means no agglomeration

Nanoparticles have different properties than bulk material because they have high surface area to volume ratio as a result of the quantum effects that start to predominate in this size range. Surface to volume ratio is inversely proportional with the particle size, hence, as the ratio increases, nanoparticles get smaller in size (Holister 2002). Decreasing particle size causes atoms on the outside of the particle will begin to dominate the ones inside the particle and changes the properties of the particle. This correlation can be seen in Figure 1.1. as it shows the percentage of surface atoms changes with the palladium cluster diameter. Increase in the ratio of surface atoms may result changes in the size range of nanometers and this lead to changes in the physical or chemical properties of the materials. High surface to volume ratio is beneficial for industry since high surface area is a critical factor for catalysts or electrodes.

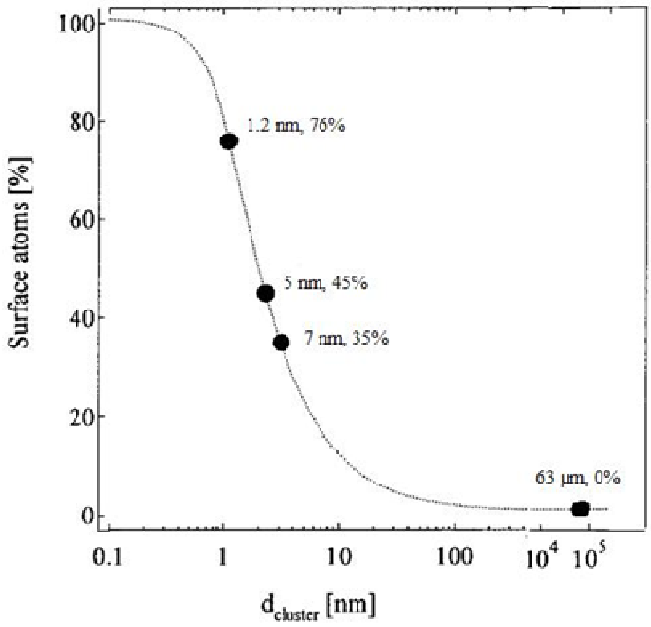

Figure 1.1. The percentage of surface atoms changes with the Pd cluster diameter (Source: Nützenadel, et al. 2000)

As mentioned before, when particle size changes from centimeter to nanometer size, their surface area increases and this increase leads to high surface energy. Higher surface energies make materials thermodynamically unstable. In order to stabilize nanomaterials, total surface energy must be decreased and overall nanomaterial size must be adjusted by preventing growth. This situation must be achieved by combining small structures to form large structures. There are several mechanisms that combine

small structures into large ones by reducing the total surface energy. The most common ones are sintering and Ostwald ripening processes. Basically, sintering is a process that uses thermal energy in order to produce density-controlled materials. It makes the particles to adhere each other. Average grain size and material densification are increased linearly with thermal energy (Kang 2005). Sintering must be achieved in order to fabricate nanomaterials, however, it only becomes predominant at high temperatures. On the other hand, Ostwald ripening process, which is the other most common phenomena, is predominant at a wide range of temperatures. It is defined as combination of individual nanoparticles to form a single one. Resulting material in sintering process is polycrystalline material, but, in Ostwald ripening process is a single material as can be seen in Figure 1.2. It is often used to get particles with a narrow size distribution because small particles are eliminated as they grow at the expense of larger particles. After initial nucleation and growth, solubility of solid in solution produces Ostwald ripening with increasing temperature. Hence, small particles are dissolved in solution because they have higher surface to volume ratio and the system tries to lower overall surface energy. Then, molecules on the surface of small particles tend to diffuse and join the surface of larger particles makes them grow in size.

Third mechanism that reduces the overall surface area, is agglomeration. In fabrication of nanostructures agglomeration is a big problem because once the particles agglomerate, it is difficult to separate them. Agglomeration occurs if high interaction between nanoparticles is present and therefore the size distribution shifts towards larger sizes.

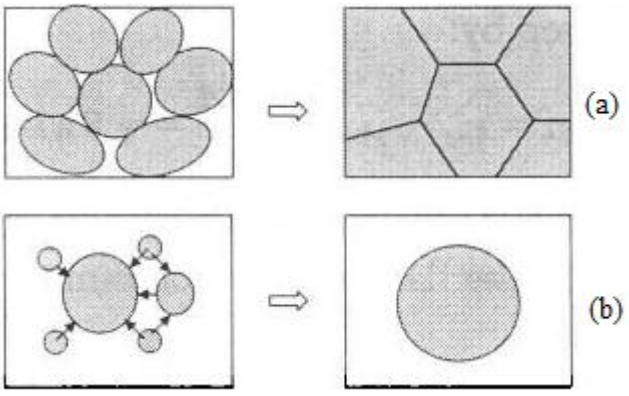

Figure 1.2. Illustration of (a) sintering process; (b) Ostwald ripening process (Source: Cao 2004)

1.1. Cerium Oxide Nanoparticles

In recent years, research on nanostructured materials have attracted great attention. Especially, cerium oxide, an important rare-earth material, is extensively studied. Cerium oxide, known as ceria or cerium dioxide, has a chemical formula of CeO_2 and it is a pale yellow powder as seen in Figure 1.3. Also, some important physical and chemical characteristics of cerium oxide are shown on Table 1.1.

Figure 1.3. Cerium oxide, is a pale yellow powder, synthesized in our laboratory.

Cerium has [Xe] $4f^2 6s^2$ electron configuration and it can show both 3+ and 4+ oxidation states. Cerium is thermodinamically unstable metal and in the presence of oxygen it can easily reduced to CeO_2 and Ce_2O_3. Generally, pressure and temperature are the major factors on the final stoichiometry. Cerium oxide, that crystallites in the fluorite structure, has face centered cubic unit cell (f.c.c) with the cell parameter of 5.410 Å, (Space group Fm3m, JCPDS 81-0792).

Table 1.1. Some important physical and chemical characteristics of bulk CeO_2 (Source: Integrated Laboratory Systems, Inc. 2006)

Chemical Name	Cerium Oxide
Formula	CeO_2
Molecular Weight	172.12 g/mol
Physical State	Solid, cubic, face-centered crystals. Solid as white, yellow or tan powders
Density	7.65 g/cm^3
Boiling Point	Not available (melts at 2500°C–2600°C)
Water Solubility	Not soluble
Refractive Index	2.0
Hardness	5–6

In a typical face-centered cerium oxide structure, each Ce^{4+} cation is formed by eight equivalent nearest-neighbour oxygen anions at the corner of a cube and each anion is tetrahedrally coordinated to four Ce^{4+} cation that is illustrated in Figure 1.4. All oxygen ions occupy tetrahedral holes of ccp array of cerium. It can be extended by drawing the oxygen atoms at each corner and each cerium at the center has eightfold cubic coordination. This clearly shows that Ce^{4+} cation occupies eight vacant coordination sites and there is a very large vacant octahedral holes in it leads to the defect structure of cerium oxide (Trovarelli 2002).

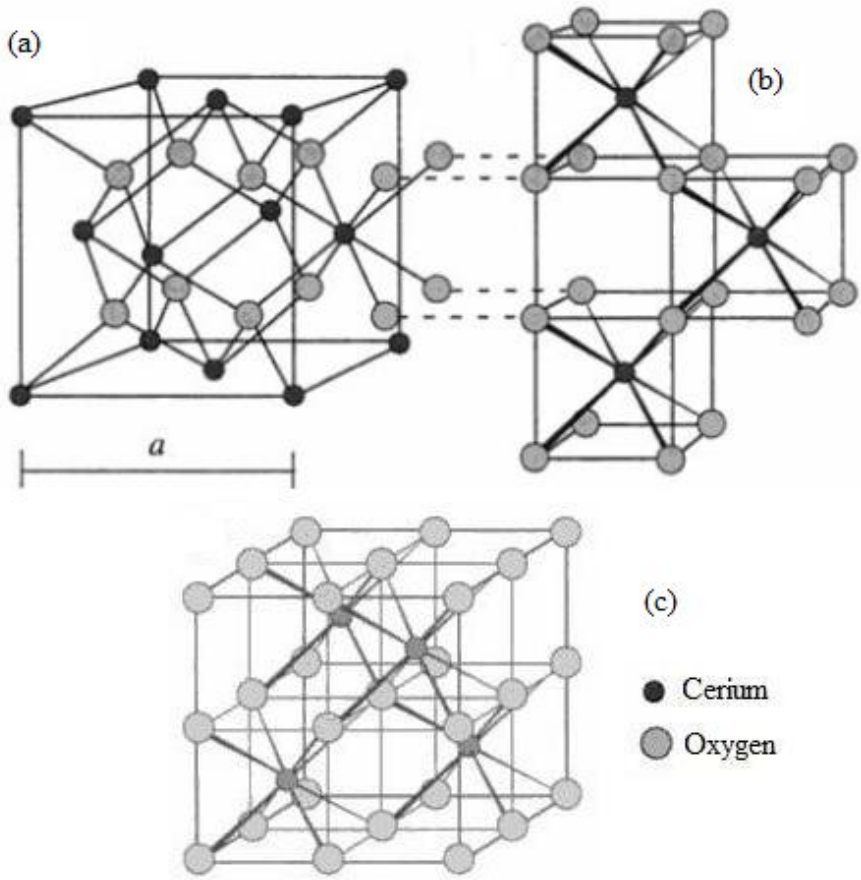

Figure 1.4. Crystal structure of cerium oxide (a) unit cell as a *ccp* array of cerium atoms and (b) and (c) the same structure redrawn as a primitive cubic array of oxygen ions (Source: Trovarelli 2002)

At first, it was determined that defect structure of non-stoichiometric cerium was in the range of Ce_2O_3-CeO_2 in which the lattice contained oxygen-vacant sites in accordance with the law of thermodynamics. Then, it was believed that removal of oxygen from fluorite cerium oxide lattice cause vacancies and defect structures were formed. Because removing one oxygen results 7-coordinated unusual symmetric cerium ions and a distorted cubic shape occurs. Despite the oxygen reduction and numerous oxygen vacancies, cerium oxide protect the fluorite structure, that's why even at low temperature reactivity of cerium towards oxygen is strong (Primet and Garbowski 2002).

1.2. Synthesis Methods

There are various techniques for production of cerium oxide nanoparticles, mainly, wet-chemical synthesis techniques such as chemical precipitation, sol-gel, microemulsion (reverse micelles), sonochemical and hydrothermal/solvothermal syntheses. Recently, Zhou, et al. (2002) produced approximately 4 nm CeO_2 nanoparticles by precipitation method, Mai, et al. (2005) obtained CeO_2 nanorods, nanopolyhedras via hydrothermal preparation, Sathyamurthy, et al. (2005) successfully synthesized CeO_2 nanoparticles with an average size of 3.7 nm by microemulsion method and Wang, et al. (2002) used both sonochemical and microwave assisted method to fabricate CeO_2 nanoparticles.

1.2.1. Chemical Precipitation Method

The process mainly occurs to form a solid substance, which is insoluble amorphous or crystalline precipitate, from a soluble reactive species in a solution. Method includes three steps that are chemical reaction, nucleation and crystal growth. In the first edition of the *Encyclopedia of Nanoscience and Nanotechnology*, Xiangdong Feng and Michael Hu noted that one of the main disadvantages of this technique is having a wide size distribution of particles because it is not a controllable process in terms of reaction kinetics, solid phase nucleation and growth processes. Besides wide size distribution, agglomeration and uncontrolled particle morphology is the other disadvantages. In order to obtain nanoparticles with a narrow size distribution the requirements of high degree of supersaturation and a uniform growth time for all particles or crystals have to be provided.

In a procedure, a solution containing metal cations are added to oxide powders to form precipitant. To improve the disadvantages of this procedure, homogeneous precipitation method has been developed. According to this process, from another chemical source of the solution, reaction participating ligands are released gradually to generate uniform precipitants throughout the solution. As an illustration, in one study hexamethylenetetramine (HMT) and urea was used in order to yield ammonia by decomposing at about 70-80°C. Therefore, the spherical CeO_2 nanoparticles, shown in Figure 1.5., with a narrow size distribution can be obtained (Chen and Chen 1993).

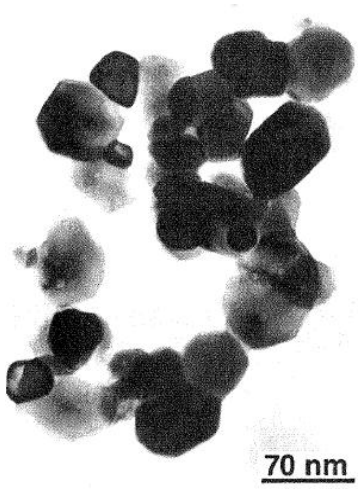

Figure 1.5. TEM image of powders prepared with Ce-HMT calcined at 450°C.
(Source: Chen and Chen 1993)

1.2.2. Sol-gel Synthesis

Sol-gel technique has been widely used to synthesize nanomaterials. In the first edition of the *Encyclopedia of Nanoscience and Nanotechnology*, Xiangdong Feng and Michael Hu noted that in this process metal alkoxides, which are dissolved in homogeneous alcohol-water solutions, are used. Technique is named sol and gel because first sol stage is developed then stage of gellation is formed.

Typically, a sol, that can be amorphous or crystalline, is a liquid phase suspension of colloidal solid particles or polymers. It is different from aerosol since aerosol is a gas phase suspensions.

A gel is a solid network, which is an agglomeration of dense colloidal particles, surrounding and supporting a continuous liquid phase. The gels are connected by means of intermolecular forces of attractions such as van der Waals forces or hydrogen bonds (Schubert and Hüsing 2000).

Figure 1.6. shows the schematic representation of the typical processing routes leading from the sol to a variety of materials. Thin films are directly prepared from sols by coating processes, powders are produced with spray-drying of sol and gelation procedure may comes after sol is cast into mold in order to give specific shape.

Resulting gel is xerogel that is obtained by drying of pore liquid. If solvent can be supercritically evacuated, it forms an aerogel (Schubert and Hüsing 2000).

Some sol-gel processes do not use alkoxides as starting precursors. Wu, et al. (2004) used porous anodic alumina template (PAA), as a complexing agent to couple the two metal species together, to produce CeO_2 nanowires with sol and gel formation.

Sol-gel processes generate mostly amorphous nanoparticles and gels if it is operated at low temperatures. Therefore, it requires further processes like calcination. In some procedures, it is coupled with hydrothermal synthesis to produce desired crystalline particles (Carnes, et al. 2002).

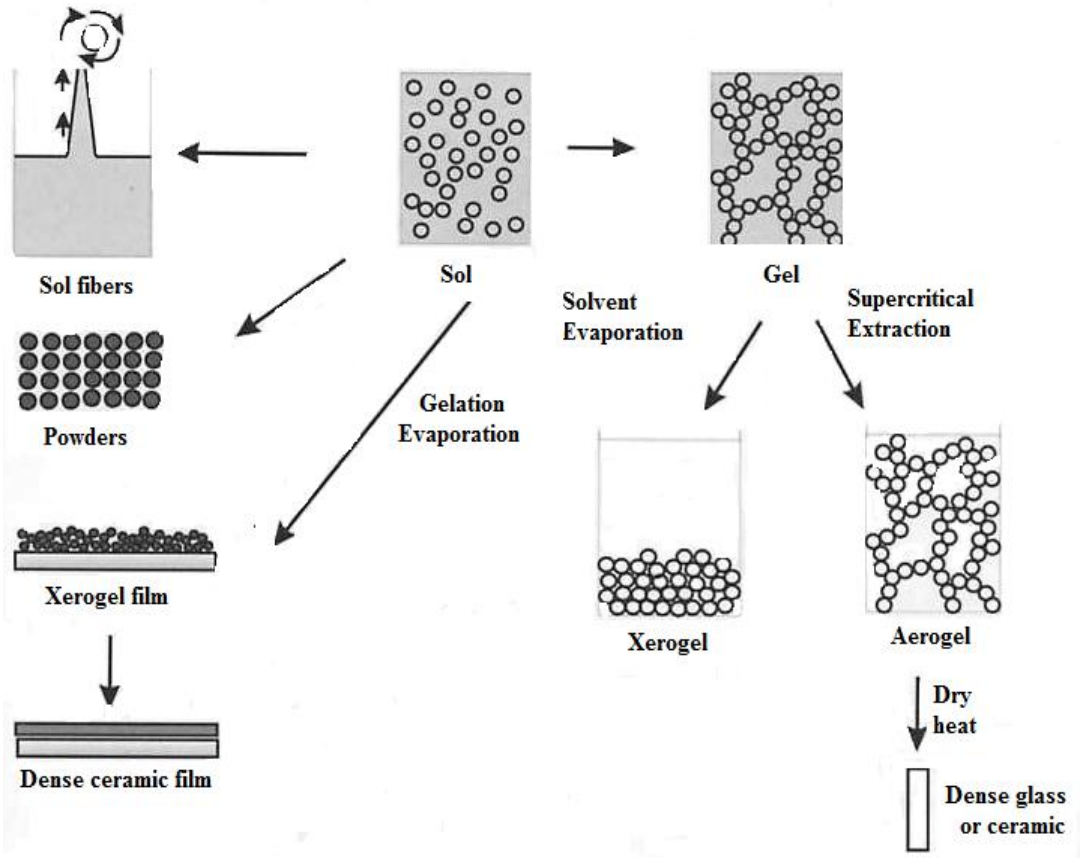

Figure 1.6. Sol-gel processing options
(Source: Schubert and Hüsing 2000)

1.2.3. Synthesis in Microemulsion (Reverse Micelles)

Typically, a microemulsion system consists of two immiscible phases, like oil-water, and a surfactant. It is well known that making one phase from two immiscible liquids cannot be possible without using a surfactant. Thus, microemulsion systems use surfactants in order to be thermodynamically stable, optically clear and usually less viscous. Low interfacial tension, large interfacial area and capacity to solubilize both aqueous and oil soluble compounds are the main characteristics of microemulsions.

There is a main difference between emulsion and microemulsion is the former is kinetically, the latter is thermodynamically stable. Stability of microemulsion depends on additives like salt, changing temperature and pressure (Paul and Moulik 2001).

Microemulsions can be classified into three (Capek 2006);

1) the oil in water (o/w) in equilibrium with oil (micelles)
2) the water in oil (w/o) in equilibrium with water (reverse micelles)
3) bicontinuous (o+w) in equilibrium with oil and water.

Generally, reverse micellar synthesis is used in literature in order to synthesize cerium oxide nanoparticles because this method gives the narrow size distribution of nanoparticles as the reaction time is limited inside the fine reverse micelles (Masui et al. 1997). Reverse micelles have spherical shapes with hydrophilic core attached to water and hydrophobic tail attached to oil on the sphere surface.

Synthesis method uses the organometallic and metal salt precursors that are dissolved inside the reverse nanosize spherical micelle water droplets. These are covered with a monolayer film of surfactant molecules. Nanoparticle formation depends on the surfactant nature (Masui, et al. 1997).

Additionally, Sathyamurthy et al. synthesized nanoparticles with using cerium nitrate and NaOH as a reaction precursors. Their microemulsion system consists of n-octane as a oil phase and cetyl trimethyl ammonium bromide (CTAB) as a surfactant that is illustrated in Figure 1.7. Hence, they obtained CeO_2 nanoparticles with an average size of 3.7 nm. Water-to-surfactant ratio is very important for these dispersions since the stability of microemulsions depends on this ratio (Sathyamurthy, et al. 2005).

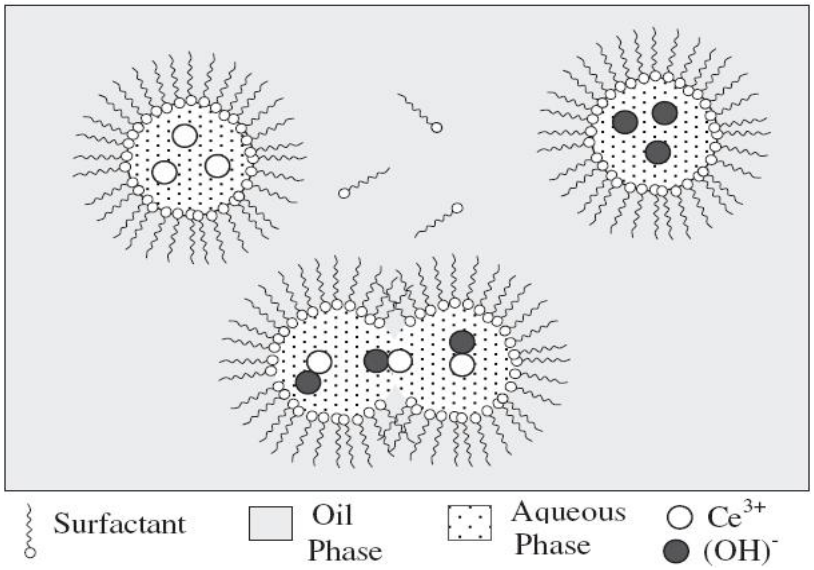

Figure 1.7. Illustration of nanoparticle synthesis using reverse micellar synthesis. (Source: Sathyamurthy, et al. 2005)

1.2.4. Hydrothermal Synthesis

1.2.4.1. History of Nanomaterial Processing With Hydrothermal Synthesis

Hydrothermal synthesis technique has become popular and gained a lot of interest over the fifteen years.

Firstly, Sir Roderick Murchison (1792-1781), British geologist, used the term hydrothermal for definition of the changes in the earth's crust and formation of rocks and minerals by monitoring the action of water at elevated temperature and pressure. A majority of minerals formed in presence of water at elevated temperature and pressure conditions are said to be "of hydrothermal origin". Therefore, in order to understand the mineral formation in nature, hydrothermal technique has been developed (Byrappa and Yoshimura 2001).

Hydrothermal synthesis on nanomaterials was carried out by Schafthaul (1845) for the first time in order to obtain nanosize quartz crystals upon transformation of freshly precipitated silicic acid in Papin's digestor. Most of early experiments dealt with nanocrystalline materials were done during 1840s to the early 1900s but faced off

failures as electron microscopic techniques were not available (Byrappa and Adschiri 2007). Therefore, bulk material fabrication became important.

Commercial application of hydrothermal chemical reaction was first performed by Karl Josef Bayer (1892) as he obtained pure aluminum hydroxide that can be converted to pure Al_2O_3 suitable for processing the metal (Goranson 1931). Today, millions of tons of bauxite ore is treated annually by the help of this process (Habashi 1994). A host of uranium ores, sulphides of gold, nickel, zinc, antimony and so on, are also treated with this process to extract the metal.

Work of Bayer was followed by Nacken (1946) with the synthesis of large single crystals and Barrer (1948) for zeolites (Nacken 1946, Barrer 1948). During World War II, demand for large size quartz crystals leaded scientists to produce large size crystals. Then, zeolite synthesis was firstly done by Barrer (1948) and from this moment molecular sieve technology was developed. The development has provided further research for hydrothermal crystal growth.

Gradually, from the late 1920s to the late 1950s, even though the wide variety of products was able to be analyzed as crystalline materials, these attempts were failed due to lack of knowledge on hydrothermal solution chemistry and kinetics of hydrothermal reactions. When high resolution scanning electron microscope is available from 1980, researchers started to analyze fine crystals. During 1990s, hydrothermal technique became popular on processing of fine to ultra fine particles with a controlled size and morphology

Recently, hydrothermal synthesis is a highly interdisciplinary subject and has not just limited to the crystal growth. It has been grown into mechanical, ultrasonic, electrochemical and microwave reactions (Roy 1994). Increasing demand on nanostructured materials lead scientists to this technique because it offers a unique method for coating various materials on metals, polymers, etc. In 21^{st} century, this technology has new perspectives that can be used by chemists, biologists, physicist, geologist and engineers as shown in Figure 1.8. (Byrappa and Adschiri 2007).

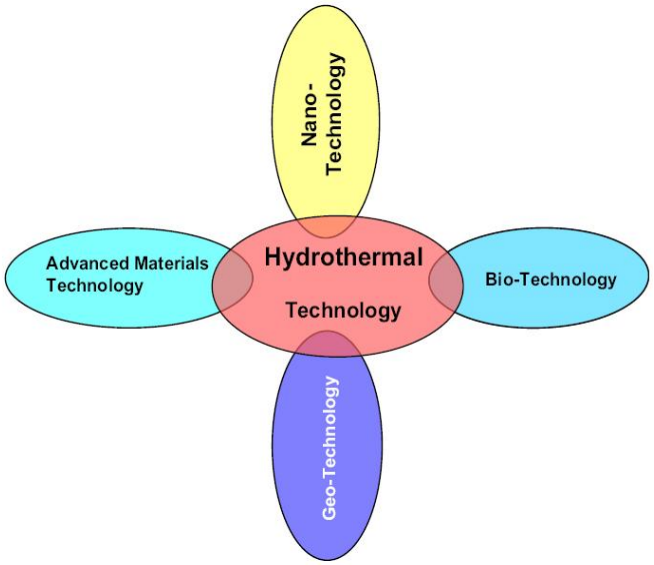

Figure 1.8. In 21st century, illustration of hydrothermal technology
(Source: Byrappa and Adschiri 2007)

Branches of science that is linked with hydrothermal technique are summarized in Figure 1.9. as in the following years, this family tree will expand in its branches and roots.

1.2.4.2. Definition and Process of Hydrothermal Synthesis

Mainly, the term hydrothermal refers to dissolve and recrystallize materials, which are insoluble under normal conditions, by applying high temperature and pressure in presence of aqueous solvent or mineralizers. The word "hydrothermal" is coming from Greek word of "hydros" meaning water and "thermos" meaning heat (Byrappa and Adschiri 2007).

There are a lot of definitions for hydrothermal synthesis in the literature. For instance, Laudise defines hydrothermal synthesis as it is the growth from aqueous solution at ambient conditions (Laudise 1970). Rabenau prefers to define it as the heterogeneous reactions in aqueous media above 100°C and 1 bar (Rabenau 1985). Most recently, Roy states that using water as a catalyst and rarely as a component of solid phases at temperatures more than 100°C and pressures greater than 1 atm is the hydrothermal synthesis (Roy 1994). Then, Yoshimura concludes that reactions carried out under high temperatures and pressures (>100°C and >1 atm) in a closed system.

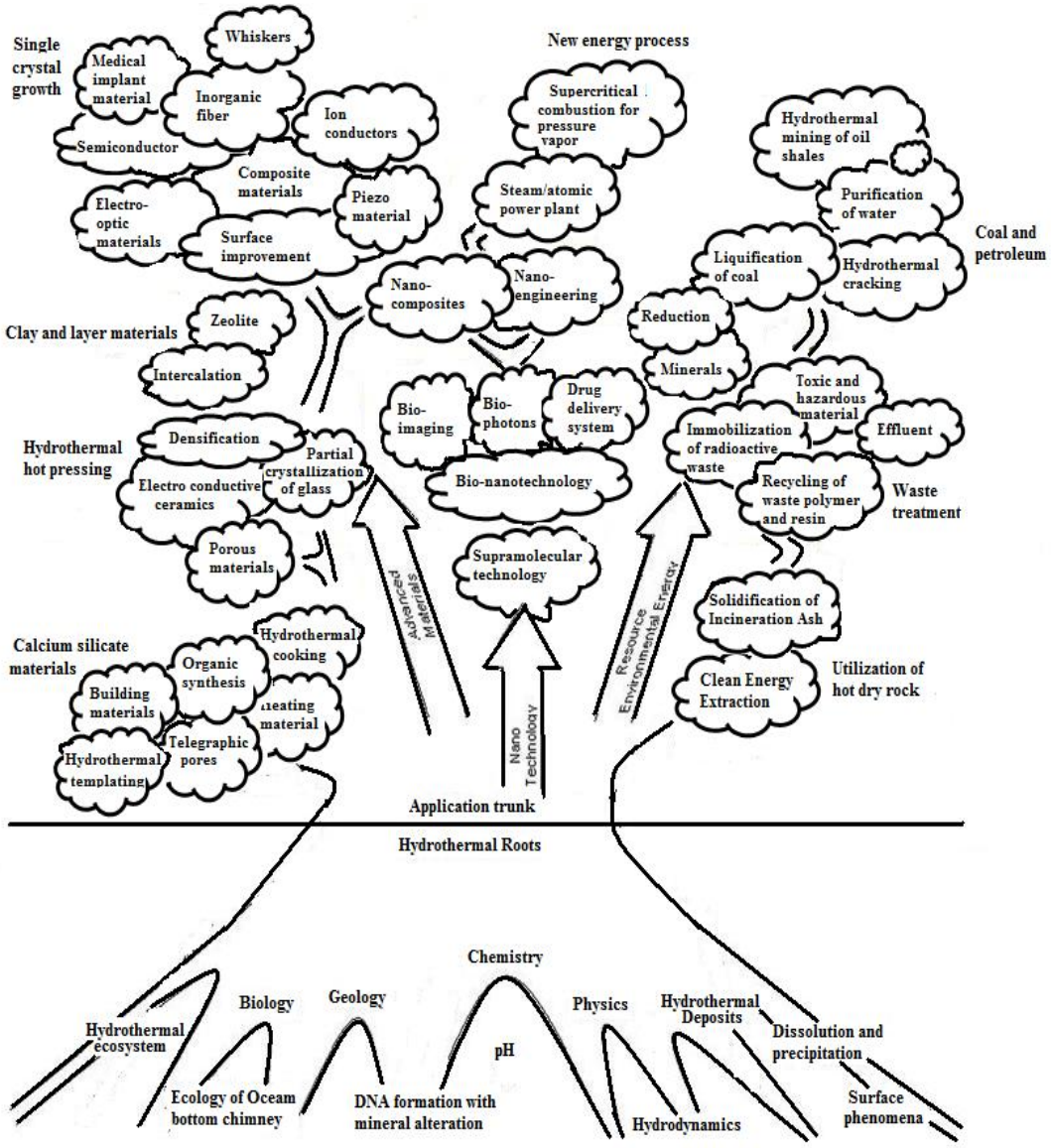

Figure 1.9. Hydrothermal tree showing different branches of science and technology (Source: Byrappa and Adschiri 2007)

It is a general thought beyond scientists that the hydrothermal synthesis takes place above 100°C and above 1 atm. However, there is no lower limit for P and T conditions. That's why hydrothermal synthesis is accurately defined as heterogeneous chemical reaction in presence of water above room temperature and 1 atm in a closed vessel (Byrappa and Adschiri 2007).

Sometimes solvothermal term is used instead of hydrothermal term. It is used when a solvent is different from water. Depending upon the solvent type the name can be glycothermal, ammonothermal, alcohothermal and so on. However, using water as a

solvent has some benefits like it minimize the pollution because it is easily volatilized and can be recycled (Komarneri 2003). Also, it is environmentally beneficial and cheaper than other solvents. By tuning the temperature and pressure, it can act as a catalyst for transformation of desired materials (Byrappa and Yoshimura 2001). Under hydrothermal conditions, it is difficult to dissolve some reactants in water and this problem can be achieved with adding mineralizers or solvents. Mineralizers speed up the reaction rate and crystal formation. They increase the compound solubility in water. The hydroxides of alkali metal salts like NaOH, KOH or LiOH, alkali salts of weak acids or elemental acids are used as mineralizers.

Hydrothermal syntheses are carried out in closed vessels and at constant volume, pressure-temperature relations of water is extremely important. Figure 1.10. shows the volume-temperature diagram of water in which volume is replaced with density. The region, in which the liquid and gas phases are at equilibrium, is said to be two-phase region. At a given temperature, density of two phases is determined by the intersections of a horizontal line. As an illustration, at 300°C, the density is 0.75 g/cm^3 for liquid phase and 0.05 for gas phase. Density of liquid phase decreases with increasing temperature, whereas, density of gas phase increases. Temperature and density of these two phases are at equilibrium at critical point that means above the critical point there is only one phase is present. That is called “supercritical or fluid phase” (Schubert and Hüsing 2000).

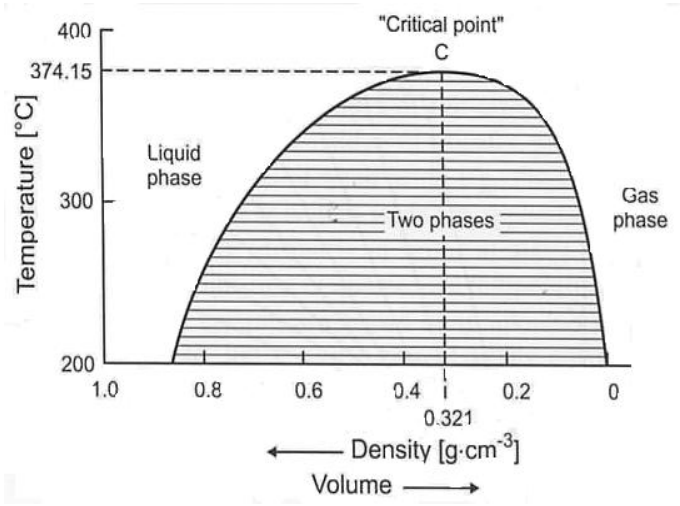

Figure 1.10. Volume (density)/temperature dependence of water
(Source: Schubert and Hüsing 2000)

During synthesis, the pressures are self-generated in which the internal expansion of a fluid with heating produces pressure without any external force. When the fluid is put in a teflon container at a low temperature with a degree of fill, it rapidly expands to fill the container at the reaction temperature. Here, degree of filling is the key parameter and ultimate pressure is determined by the initial room temperature fill. This can calculated by using P-T tables shown on Figure 1.11. in which T_r represents triple point (solid-liquid-gas phases coexist) and C represents critical point.

Generally, it is found that fills more than 32% initially, at temperatures below critical point (373°C), the liquid begins to fill the whole autoclave. Because increasing temperature causes to raise the meniscus between gas and liquid phase. For instance, if the initial percentage filling of autoclave is 80%, then the whole autoclave is filled with liquid at approximately 245°C that is below the critical temperature. If autoclave is filled 32% exactly, liquid level remains unchanged until critical temperature. Filling less than 32% cause decreasing of the level of liquid and below critical temperature one phase coexist that is gas phase (Schubert and Hüsing 2000). Generally, increasing percentage of fill causes decreasing the temperature of autoclave filling with water.

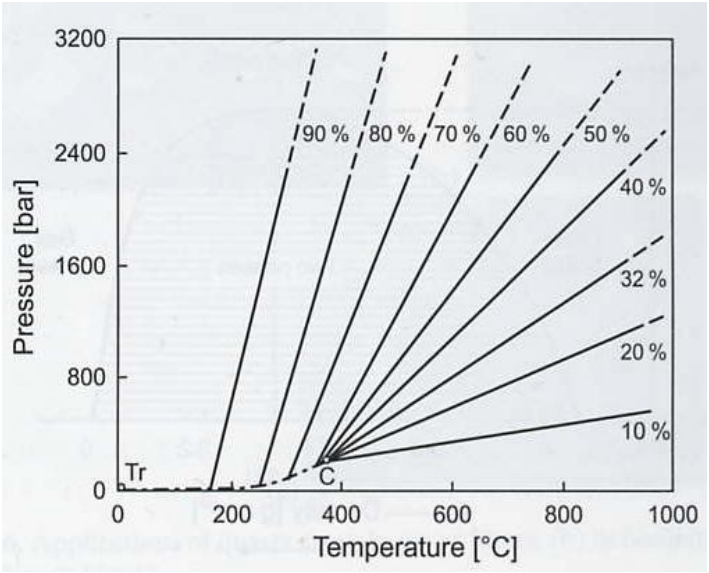

Figure 1.11. PT dependence of water for different degrees of filling of the vessel (Source: Schubert and Hüsing 2000)

As a conclusion, hydrothermal technique has some advantages over conventional synthesis techniques. Firstly, even at low temperatures, desired crystalline materials can be directly synthesized and like in sol-gel processing calcination step do not require. Moreover, controlling particle size and morphology is easy in hydrothemal synthesis by changing the conditions like pH, temperature or nature of surfactant. Finally, resulting materials can be used directly in steps like filtration (Kaya, et al. 2002).

1.3. Applications of Cerium Oxide Nanoparticles

Cerium oxide is a very important rare-earth material and it has a high oxygen ion conductivity and oxygen storage capacity (Campbell and Peden 2005). These properties make cerium oxide useful for applications such as an electrolyte material in solid oxide fuel cells (Stambouli and Traversa 2002) and as a catalyst material (Trovarelli, et al. 1999). Also, it can be used in the area of polishing powders (Kosynkin, et al. 2000), UV-blockers (Imanaka, et al. 2003) and gas sensors (Khodadadi, et al 2001).

Generally, pure ceria is doped with different cations in order to use in applications. Doping different cations stabilize cerium oxide against sintering and it can be used at high temperatures without reducing its oxygen storage capacity and thermal stability. As an illustration, addition of zirconium in the formation of ceria-zirconia solutions is effective (Suda, et al. 2008). Doping also increases the number of oxygen vacancies and this property provides high oxygen storage capacity.

CHAPTER 2

EXPERIMENTAL METHOD

2.1. Reaction Autoclaves

Reactions under hydrothermal conditions require a closed vessel that is durable to high temperatures and pressures. This closed vessel is named as an autoclave and an ideal autoclave must meet the following characteristics:

a. Inertness to acids, bases and oxidizing agents.
b. Leak-proof with unlimited capabilities to the required temperature and pressure.
c. Long-time duration, so that, no machining or treatment is needed after each experimental run.

During this study, PTFE (polytetrafluoroethylene)-lined acid digestion bombs illustrated in Figure 2.1. are used as reaction autoclaves. These are purchased from Parr Instrument Company (Illinois, USA) and removable Teflon is used as a lining material. Especially, experiments are done under mild hydrothermal conditions, in which the operating temperature is maximum 250°C and maximum pressure is 1800 psi, Teflon is the most popular lining material. Because it has a larger coefficient of thermal expansion versus the material in which it is enclosed. Upon heating and cooling, the Teflon material expands, so, it is useful to maintain a constant pressure on Teflon by a spring loaded closure (Byrappa and Yoshimura 2001).

Pressure during the hydrothermal synthesis with these autoclaves depends on the nature of the solution, the degree of filling and the temperature. When the operating temperatures are more than the limits of the autoclave, it causes to increase the vapor pressure of the solution and to decrease the durability of materials that an autoclave is made of. Furthermore, the solutions tend to expand and fill a space 25% larger than its standard value. There must be sufficient vapor space in the autoclave so that it does not totally liquid full and increasing hydrostatic pressure will not destroy it.

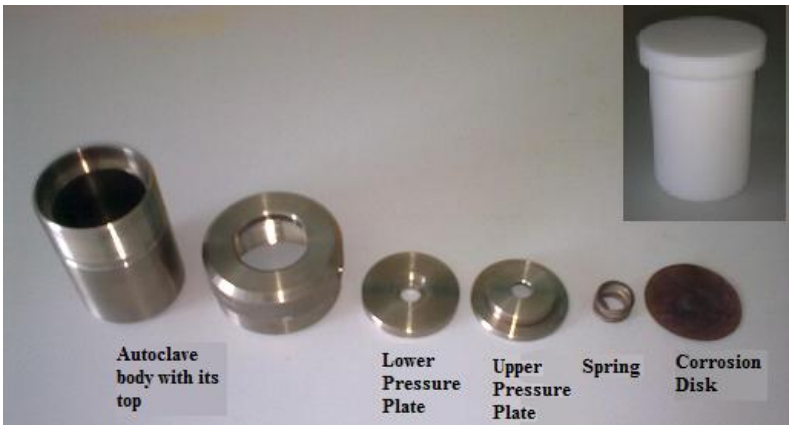

Figure 2.1. Schematic representation of an autoclave with its parts. (Inset shows the Teflon liner)

23 mL Teflon lined reaction autoclaves (Parr Instruments – model 4749) are used during the hydrothermal treatment. After adding the precursor materials to the Teflon liner, it was placed in an autoclave covered first corrosion and rapture disks. Then, the spring with upper and lower pressure plates were placed. Finally, with a screw cup was firmly closed.

2.2. Experimantal Procedure

2.2.1. Synthesis

In a typical synthesis that is illustrated in Figure 2.2., 0.5 g $Ce(NO_3)_3 .6H_2O$ was dissolved in a 3 mL of water and 15 mL of alkali base solution was added. Pale yellow amorphous CeO_2 was precipitated and after 30 minutes stirring at room temperature, mixed slurry was transferred into 23 mL autoclave and hydrothermal synthesis technique was applied for different reaction times and temperatures. Autoclaves were allowed to cool slowly to room temperature and product was washed with water and centrifuged at 6000 rpm and dried at 60°C for further characterization (Yang, et al. 2007).

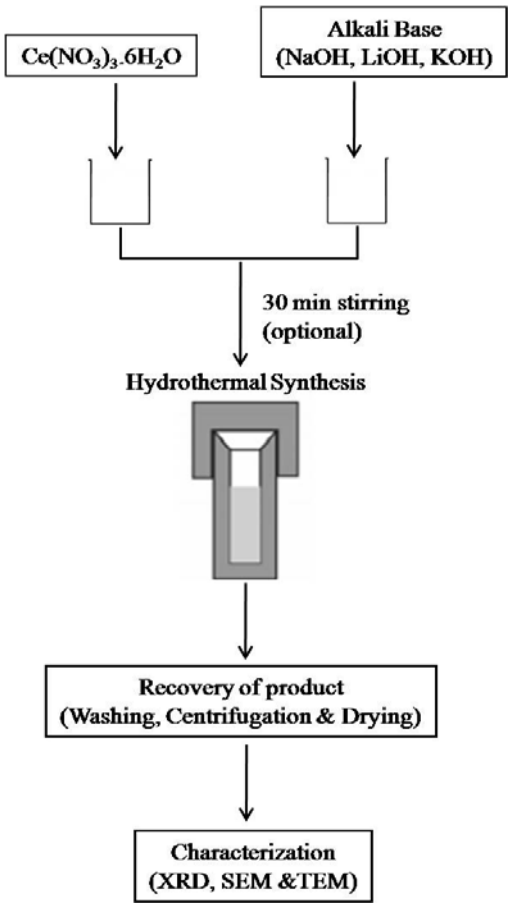

Figure 2.2. Block diagram of the procedure used during the synthesis

2.3. Characterization Techniques

After successfully fabrication of cerium oxide nanoparticles, characterization is the most important part of the research. Because it is definitely important to know the structure and composition of synthesized material. First researchers, who deal with the synthesis of nanomaterials, had difficulties about measuring and manipulating of their materials because of the lack of microscopic techniques. A better fundamental understanding and potential applications, demand for instrumentation has increased.

Characterizations of nanomaterials require both sensitivity and accuracy. Atomic-level resolution is also important for characterization. Hence, microscopic techniques are the heart of characterization and measurements of nanomaterials.

Typically, identification of cerium oxide nanoparticles is done with the method of X-ray diffraction because if a molecular is crystalline, its identification is usually done with this method. Each crystalline material has its own characteristic X-ray

powder pattern and this can be used as a fingerprint for its identification. By the help of matching with known materials, unknown materials can be found easily.

The next step after identification is the structure determination that is easily done with the help of microscopic techniques such as Transmission Electron Microscopy (TEM) and Scanning Electron Microscopy (SEM).

Also, spectroscopic techniques help to determine the optical properties of nanomaterials especially for semiconductor materials. Cerium oxide is a semiconductor material and its optical properties can be determined by using UV-VIS Spectroscopy and Fluorescence Spectroscopy. One advantage of these techniques as they are inexpensive and provide fast data acquisition.

It must be known that no single technique is capable of providing a complete characterization of a solid. Characterization techniques of crystalline nanoparticles can be divided into two, structural characterization and optical characterization.

2.3.1. Structural Characterization

2.3.1.1. X-ray Diffraction

X-ray diffraction (XRD) is a powerful technique for investigation of crystal structure of a solid with lattice constants and geometry. It is also used for identification of unknown solids, orientation of single crystals and orientation of defects in crystal structure (Cao 2004).

In electromagnetic spectrum, x-ray region is defined with a wavelength of approximately 0.5-2.5Å. Figure 2.3. shows a typical instrumentation of X-ray diffraction. X-rays are produced in X-ray tube by colliding a high speed electron with a metal target under the high voltage system. When produced beam of X-rays fall on a specimen, they are diffracted by the crystalline phases in the specimen according to the Bragg's law:

$$n\lambda = 2d \sin\theta \tag{2.1}$$

where n is the order of reflection, λ is the wavelegth of incident x-ray, d is the interplanar spacing between planes of a crystal and θ is the angle between incident beam and specimen surface (Cullity 1978).

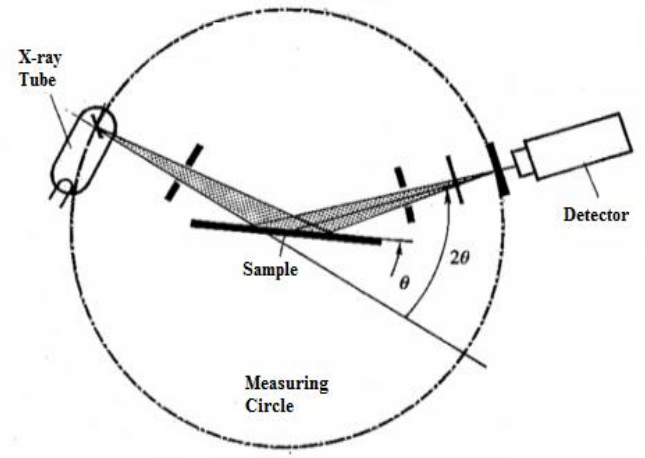

Figure 2.3. The X-ray Spectrometer.
(Source: Smart and Moore 1996)

Diffracted x-ray intensity is measured as a function of the diffraction angle, 2θ and the specimen's orientation. This diffraction pattern is used to get information about the structural properties and to identify the specimen's crystalline phases. It is a set of lines or peaks that has different intensity and position. These intensities are charactrestic property of a material. Figure 2.4. shows a typical x-ray diffraction pattern of cerium oxide.

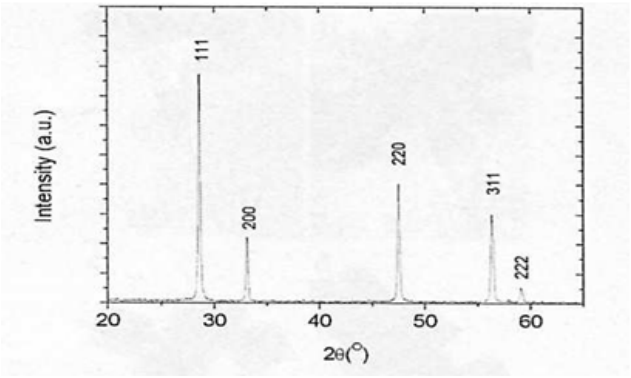

Figure 2.4. Typical XRD spectrum of cerium oxide nanoparticles
(Source: Yang, et al. 2007)

After diffraction pattern is obtained, it is compared with the known published patterns. If a substance is a common type, it matches one of the known patterns. Standard patterns of crystalline substances are given in the powder diffraction file, JCPDS (Joint Committee on Powder Diffraction Standards). This database contains more than 35000 entries and it increases every year. If powder diffraction pattern has never been collected before, some hypotheses can be made on structural type (Smart and Moore 1996).

Average crystallite size (D) measurements can be done with using x-ray diffraction pattern with applying Debye Scherrer's formula to the most intense peak:

$$D = \frac{0.9\lambda}{B\cos\theta_B} \tag{2.2}$$

where λ is the wavelength of radiation, B is the full width at half maximum (FWHM) of the Bragg peak on the 2θ scale in radians and θ_B is the Bragg angle. Peak broadening occurs due to the nano scale nature of crystal structure and this formula calculates peak broadening in terms of crystallite size. However, it should be noted that Scherrer's formula can produce different results from the true particle sizes because of forming twinned nanostructures. Besides, X-ray diffraction uses only a small amount of powder and it only provides the collective information of the particle sizes (Cao 2004).

In this study, X-ray powder diffraction (XRD) measurements were done with Philips X-pert Pro Powder Diffractometer with CuKα radiation. (λ=1.5406 Å) X-ray source is the Philips high intensity ceramic sealed tube and data was collected for 2θ values of 20° to 60°.

2.3.1.2. Scanning Electron Microscope (SEM)

Scanning elctron microscope (SEM) is generally used to investigate the surface morphology and structure composition. It has high resolution down to a few nanometers and fast scan rates and magnifications that can be adjusted from approximately 10 to over 300000. One drawback of this technique is that the requirements of expensive high vacuum environment as well as the used material need to be conductive.

Basically, its working principle depends on using electrons instead of light in order to image a sample. Electrons are produced at the top of the microscope which is

an electron gun generally made of tungsten filament. Then, these electrons are focused into a beam with a very fine spot size of ~ 5 nm. Electron beam follows a vertical path, it makes its way through lenses. Once they strike and penetrate the surface, electron-specimen interactions, like emission of electrons and photons from sample, are occurred. Detectors collect the emitted electrons and convert them to a signal (Cao 2004).

In order to determine the chemical composition of a specimen, SEM is coupled with the energy dispersive x-ray detector (EDX). A computer stores the energies of x-rays from all the elements and it controls the EDX system. Simply, it identifies the element by giving rise to a line in spectrum. Hence, qualitative analysis is done rapidly. However, EDX has some limitations like it cannot detect elements lighter than sodium and the energy resolution of the detector is poor that means each x-ray line cannot be detected accurately (Goodhew, et al. 2001).

2.3.1.3. Transmission Electron Microscope

Transmission electron microscope (TEM) is probably the best technique to investigate the morphology because it has high magnification ranging from 50 to 10^6. Also, it can provide both image and diffraction information from a single sample. Figure 2.5. shows the size scale with respect to some objects of specific interest and the microscopes that are needed to image them.

In TEM, an electron beam is accelerated to 100 keV or higher and it is transmitted through an ultra-thin specimen. It interacts with specimen then the image is formed and magnified by lenses onto the screen. Adjusting the strength of lenses, image of a sample is easily converted to its electron diffraction pattern. As mentioned before, TEM has higher resolution from other microscopes. This feature is coming from small de Broglie wavelength of its electrons and allows the instrument to detect every fine detail. As an illustration, electrons that have 0.37 nm wavelengths and 100 keV energies are able to penetrating through 0.6 μm of silicon. It is possible to work with thicker samples when the operating voltage is high because resolution is increased and electrons having high energy interact less strongly with matter (Cao 2004).

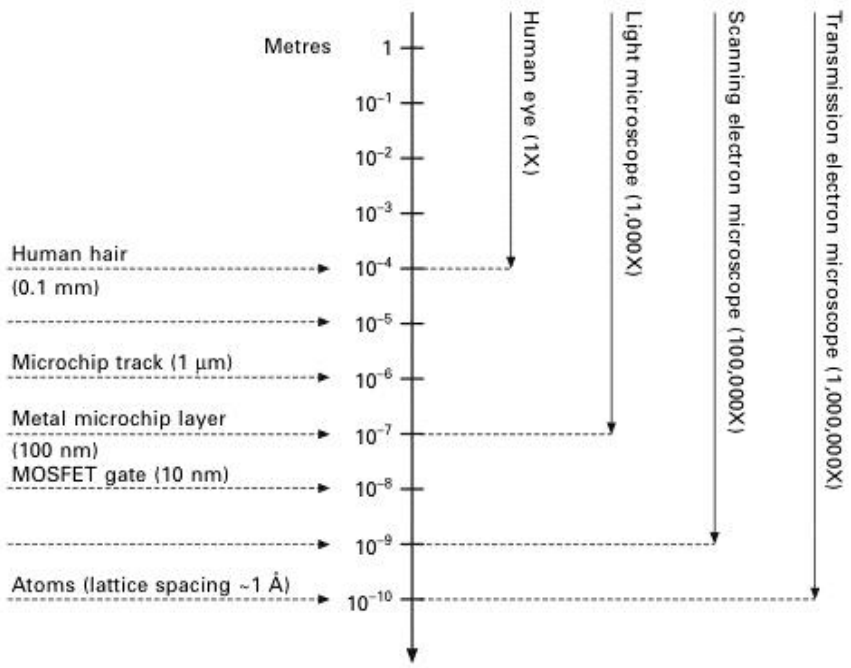

Figure 2.5. The size scale with respect to some objects and the microscopes that are needed to image them. (Source: Hannink and Hill 2006)

Selected area electron diffraction (SAED) is used to determine the crystal nature of materials like in x-ray diffraction. SAED can be made by using an aperture lower down the column, in plane of later intermediate images. This aperture is called "diffraction aperture" and it limits the diffraction volume. When looking at the diffraction patterns of materials, the one can easily understand the material crystallinity and lattice spacings.

Surface morphology measurements were done with a Philips XL 30S FEG Scanning Electron Microscope. Accelerating voltage was 5 kV and detector type was secondary electron. Transmission electron microscope was also used. The analyses were done at Max Planck Institute in Germany with a TEM FEI Tecnai F-20 microscope.

2.3.2. Optical Characterization

Optical spectroscopy is widely used in characterization of nanomaterials and it can be classified as absorption and emission spectroscopy. The former relates with absorption that is a process of exciting electrons of an atom, ion or molecule from

ground to the excited states and the latter deals with emission that is a relaxation process of an electron from excited to ground states.

2.3.2.1. UV-Vis Spectroscopy

Ultraviolet-Visible (UV-Vis) spectroscopy concerns the light in the UV-Vis range (180-780 nm). In this region, molecules undergo electronic transitions and color of a solution affects the absorption in the visible range. Increasing number of molecules, that absorb light of a given wavelength, also increases the extent of light absorption. That is the main principle of this technique. From this principle, Beer-lambert law is developed:

$$A = \varepsilon bc \tag{2.3}$$

where A is the absorbance, ε is the molar absorptivity, which is known as a property of the molecule undergoing an electronic transition, b is the length of sample (cm) and c is the molar concentration of solute. If a molecule has observed absorption, it can be said that the molecule obeyed Beer-lambert law (Pavia, et al. 2001).

Cerium oxide nanoparticles are semiconductor nanoparticles that show strong absorption below 400 nm with a well-defined absorption peak around 300 nm and block damage by UV radiation. While a semiconductor absorbs light, an electron moves from valance band to the empty higher conduction band and leaves a hole (electron vacancies) behind. Bandgap, which is between the valance and conduction band, prevents the flow of electrons. This flow of electrons relates with conductivity and it increases with the temperature (Miessler and Tarr 2003). Bandgap is indicated by a blue shift in the absorption edge and by the discrete electronic transitions as the nanoparticle gets smaller in size.

For cerium oxide nanoparticles, the bandgap energy can be determined from UV-Vis spectrum with cutting the wavelength axis by extrapolating the absorption peak. In literature, bandgap values of cerium oxide nanoparticles are varied. For instance, Yu, et al. (2004) have reported a bandgap value of 3.7 eV for hydrothermally prepared cerium oxide nanoparticles in presence of block-co-polymers. Furthermore, Yin, et al. (2002) have found this value can be in a range from 3.03 to 3.68 eV for sonochemically synthesized cerium oxide nanoparticles. Another approach has been

developed by Masui, et al. (1997) as they were synthesized cerium oxide nanoparticles with reverse micellar synthesis and they found a range from 3.38 to 3.44 eV.

2.3.2.2. Fluorescence Spectroscopy

When a material gains energy from a light source, it absorbs photons at some wavelength and promotes an electron from a ground state to a higher energy level. This process can be desribed as a transition from ground state to excited state of an atom or from the valance band to the conduction band of a semiconductor crystal or polymer.

The system then undergoes a relaxation that means excited electron will return to the ground state, after a characteristic lifetime in excited state. This whole process is called fluorescence. In fluorescence, the wavelength of the emitted light is longer than the incident light (Cao 2004). A plot of emission against wavelength for any given excitation wavelength is called as the emission spectrum.

Rare-earth ions have typical line spectra based on intra-4f transitions. Fluorescence spectra is related to 4f-5d transitions and they are involved broad spectral linewidth that are crystal field related and can be tuned by the size and crystal structure (Yan and Yan 2008). Cerium oxide nanoparticles give strong emission peak around 400 nm and their spectrum has particle size dependent shifts. The morphology dependent feature, size and defect level effect the fluorescence spectrum of cerium oxide nanoparticles can be investigated.

Optical properties were investigated using Varian Cary 50 UV-Vis Spectrometer and Varian Cary Eclipse Fluorescence Spectrometer under excitation at 290 nm at room temperature.

2.4. The Purpose of the Study

The main purpose of this study is first to synthesize cerium oxide (CeO_2) nanoparticles via hydrothermal method and then to determine the controlling parameters, such as alkali type, alkali concentration, reaction temperature and reaction time on structure and size of CeO_2 nanoparticles. Afterwards, the optical properties of CeO_2 nanoparticles are examined.

CHAPTER 3

RESULTS AND DISCUSSION

3.1. Morphological and Structural Characterization

Figure 3.1. illustrates the typical XRD pattern of CeO_2 nanoparticles prepared in the presence of different alkali bases. XRD pattern (with CuKα) shows well defined characteristic reflections of CeO_2 and all reflections were indexed to a cubic fluorite structure (JCPDS – 81-0792) with a lattice parameter of 5.412 Å. Powder pattern shows the absence of Ce^{3+} defect states in CeO_2 nanoparticles. Cerium oxide has a mixed valance cations in bulk structure and reduction of the valance from 4+ to 3+ causes to increase lattice constant and to decrease electrostatic forces between particles (Tsunekawa, et al. 2000).

Defect state relates to the oxygen vacancies and specific control of the oxygen spacing will be used in many applications. Migration and formation of oxygen vacancies relate to the oxygen storage capacity. Materials having high oxygen storage capacity are more efficient in fuel cells (Yang, et al. 2004).

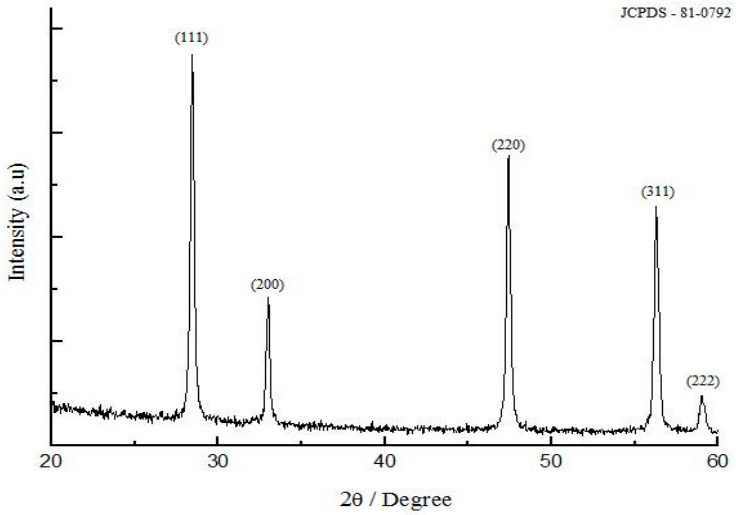

Figure 3.1. XRD pattern of as-prepared CeO_2 nanoparticles.

Morphology of CeO_2 nanoparticles were investigated using SEM and TEM. According to SEM results cerium oxide nanoparticles have uniform cubic shape. EDX spectrum in Figure 3.2 shows the presence of Ce and O element in the product.

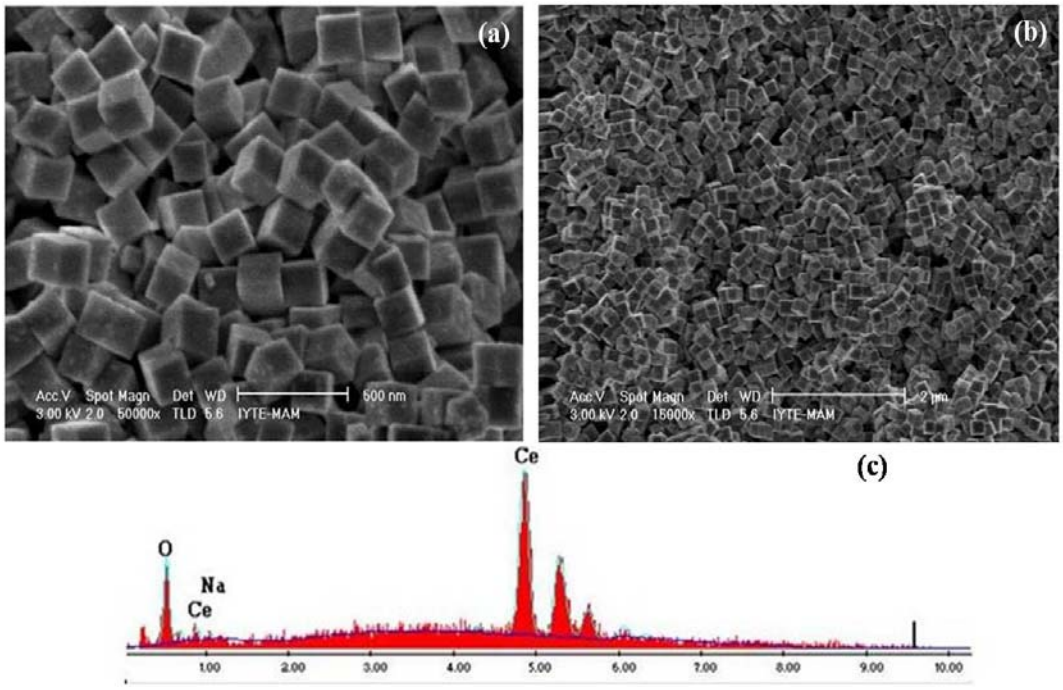

Figure 3.2. (a) and (b) SEM images, (c) EDX spectrum of cubic CeO_2 nanoparticles prepared at 240°C for 24 h in presence of 8M NaOH.

TEM images in Figure 3.3. show single CeO_2 cube synthesized with LiOH alkali base and it is composed of well crystallized nanosized grains with the clear view of lattice fringes. From high resolution TEM image, it can be easily seen that no atomic defect is present. Studies on defects of CeO_2 showed that the fluorite crystalline nature of a material remains unchanged over a wide range of nonstoichiometric compositions through the containing oxygen vacancies (Morshed, et al. 1997). The crystalline nature of resultant CeO_2 nanocubes can also be verified by selected area electron diffraction (SAED) pattern which is taken from an area of 21 nm in diameter. SAED pattern is basically a ring pattern and can be indexed, as in XRD pattern, using fluorite structure.

Figure 3.4. presents TEM images of CeO_2 synthesized using LiOH from different angles proving three dimensional cubic structure of the CeO_2 nanocrystals.

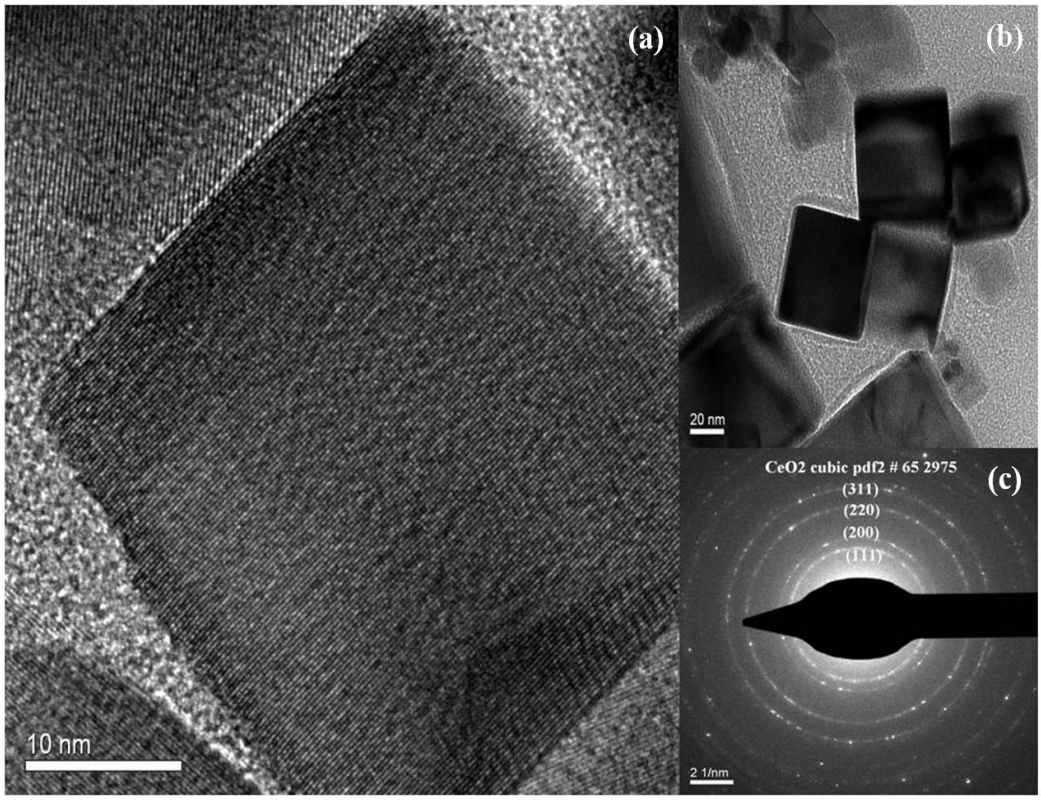

Figure 3.3. (a) HRTEM image of a single CeO_2 nanocube synthesized at 240°C for 24 h. in presence of LiOH. Insets show (b) TEM image of cubic nanoparticles and (c) SAED pattern.

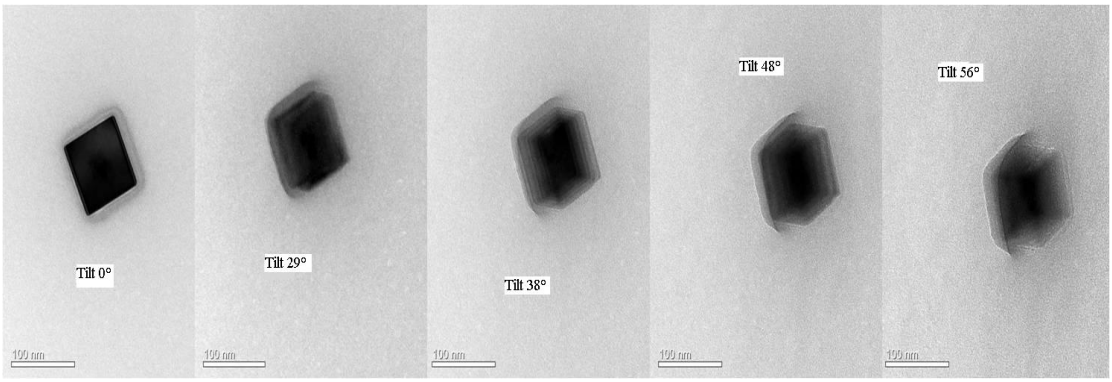

Figure 3.4. TEM image of single CeO_2 nanocube tilted along several projections. The heating temperature was 240°C for 24 h.Used base was LiOH.

3.2. Controlling Factors on Size and Shape of CeO_2 Nanoparticles

It has proven that alkali type and concentration, reaction temperature, reaction time effects significantly both size and shape of nanoparticles.

3.2.1. Effects of Alkali Base Type and Concentration

Firstly, effect of different alkali concentration was investigated with LiOH base. Keeping the temperature constant and varying the concentration of LiOH leaded to not only morphological changes, but also size changes as can be seen in Figure 3.5. High monomer concentration results in branched structures like cubic shape (Peng 2003).

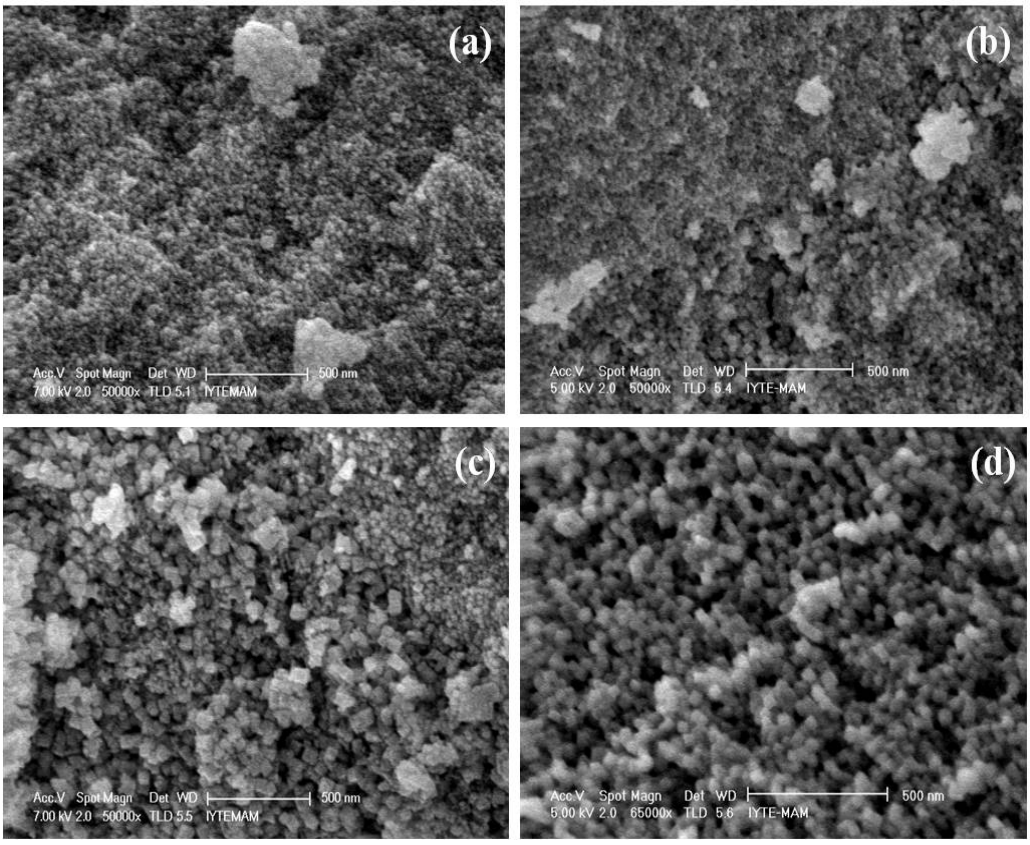

Figure 3.5. SEM images of obtained CeO_2 nanoparticles. Precipitated at 240°C for 24 h. Used base was (a) 0.1 M LiOH, (b) 0.5 M LiOH, (c) 5M LiOH and (d) 8M LiOH.

Variation of concentration was performed for KOH and NaOH as well. As in Figure 3.6. and Figure 3.7., concentration dependence of particle size was also observed for these alkali bases.

XRD patterns in Figure 3.8. for LiOH showed that as the concentration was increased, peaks of CeO_2 became intense and sharper. Same results were obtained with NaOH and KOH alkali bases. Generally, wider the XRD peak, lower the crystallite size of nanoparticles (Lian, et al. 2004).

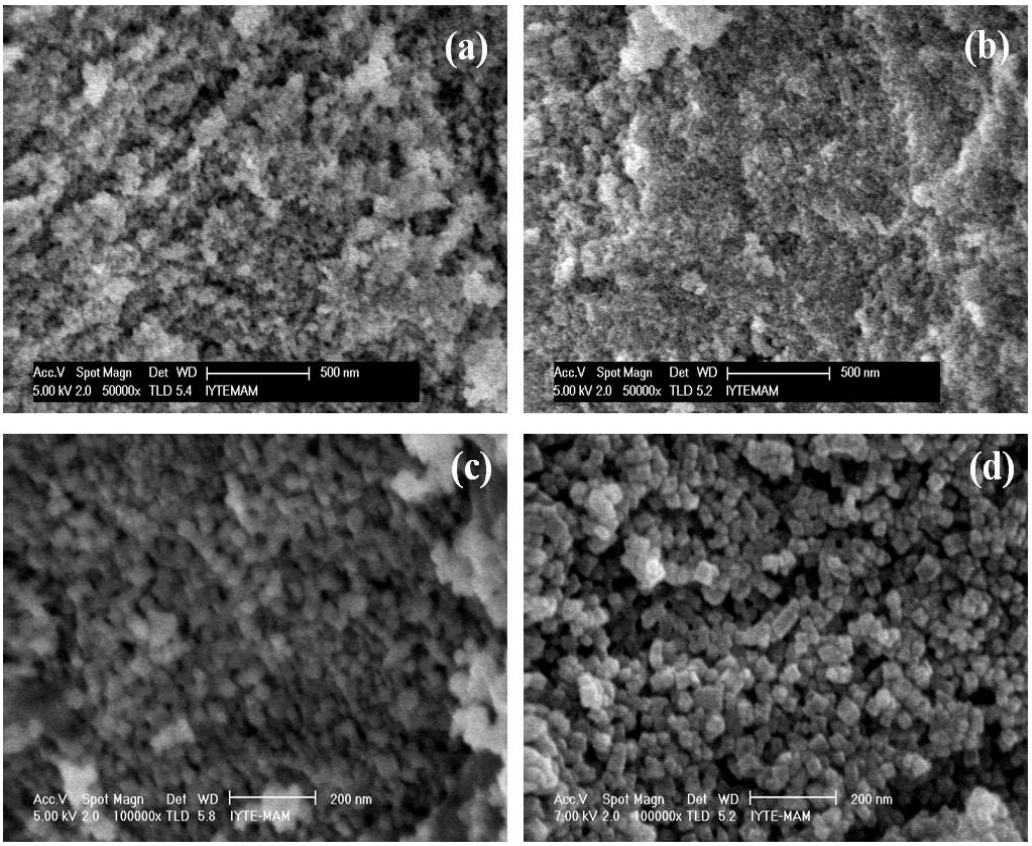

Figure 3.6. SEM images of obtained CeO_2 nanoparticles. The condition was 240°C for 24 h. Used base was (a) 0.1 M KOH, (b) 0.5 M KOH, (c) 5M KOH and (d) 8M KOH.

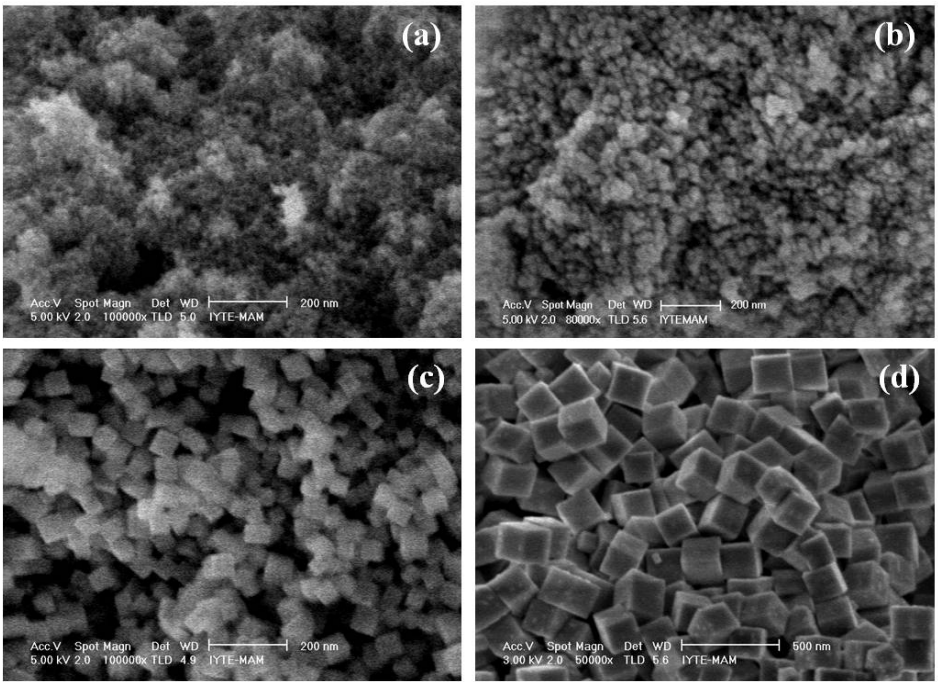

Figure 3.7. SEM images of obtained CeO_2 nanoparticles. The condition was 240°C for 24 h. Used base was (a) 0.1 M NaOH, (b) 0.5 M NaOH, (c) 5M KOH and (d) 8M NaOH.

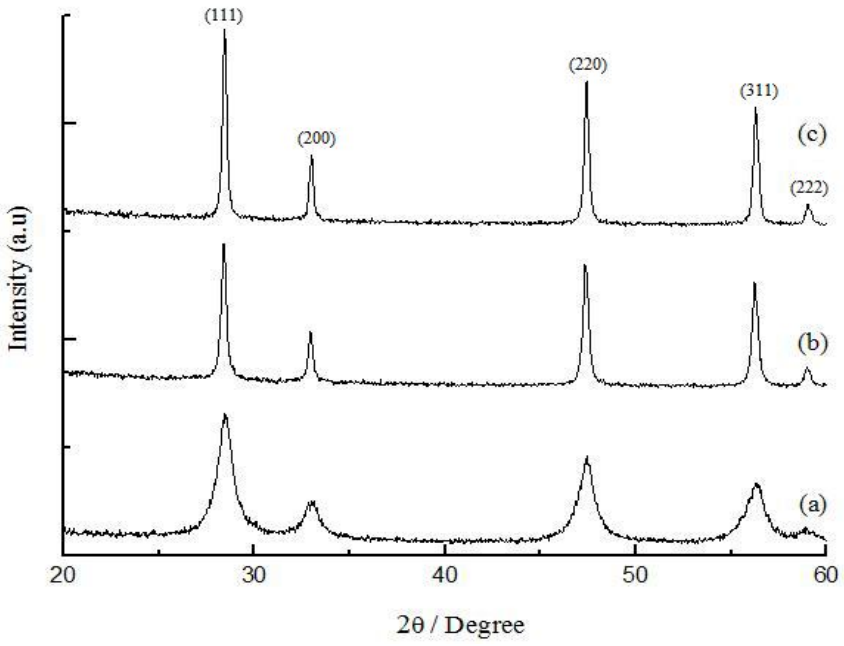

Figure 3.8. X-ray diffraction patterns of CeO_2 nanoparticles prepared at 240°C for 24 h. (a) 0.1 M LiOH, (b) 5M LiOH and (c) 8M LiOH.

When alkali base type is changed, significant changes occur in the formation of CeO_2 nanoparticles. KOH, NaOH and LiOH from 1A group of periodic table were investigated. Structural determinations were done again with SEM and TEM. SEM images are shown on Figure 3.5., Figure 3.6. and Figure 3.7. respectively.

From TEM images of three different alkali bases, it can be clearly seen that we obtained cubic cerium oxide nanoparticles successfully. Also, SAED patterns are consistent with each other and XRD patterns. Lattice fringes were calculated and they were close to the interplanar spacing in XRD measurements. The results are shown on Table 3.1. TEM images are shown on Figure 3.3. for LiOH, Figure 3.9. for KOH and Figure 3.10. for NaOH.

XRD patterns for these alkali bases are shown in Figure 3.11. When moving up a 1A group on the periodic table, XRD peaks get sharper and more intense. This indicates the increasing crystallite size and the atomic radius dependence of crystallite size. Average crystallite sizes were determined by applying full width half maximum (FWHM) to the most intense (111) peak using Debye Scherrer equation described in section 3.3.1.1. Results are shown in Table 3.2.

Table 3.1. Calculated lattice fringes from SAED and interplanar spacings obtained from XRD.

	Lattice Fringes (nm)	d (nm)
LiOH	0.2170	0.2252
NaOH	0.2273	0.2252
KOH	0.2273	0.2252

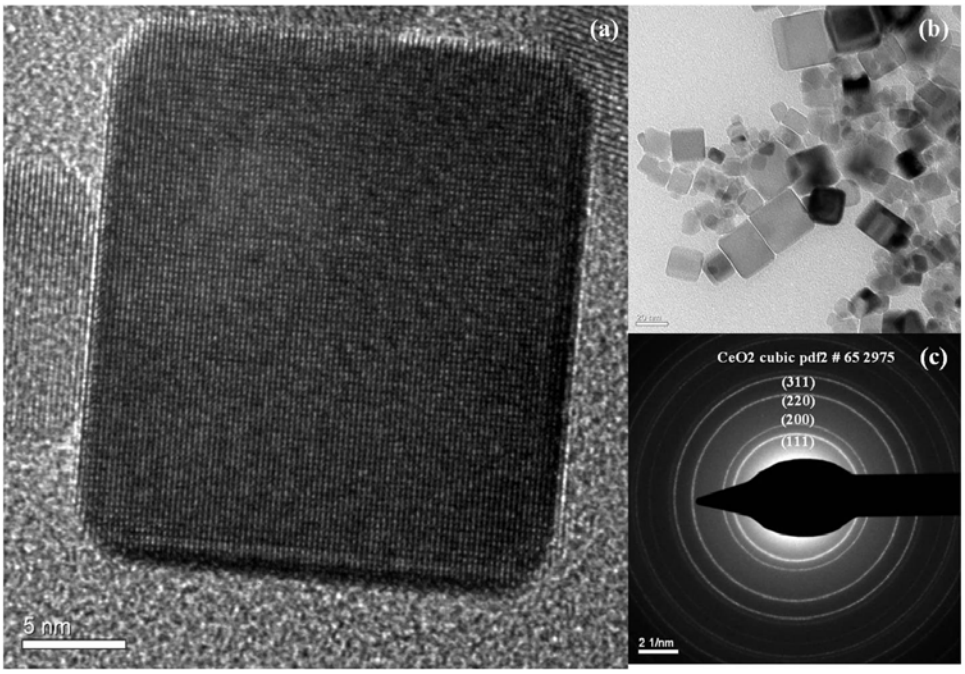

Figure 3.9. (a) HRTEM image of a single CeO_2 nanocube synthesized at 240°C for 24 h. in presence of KOH. Insets show (b) TEM image of cubic nanoparticles and (c) SAED pattern.

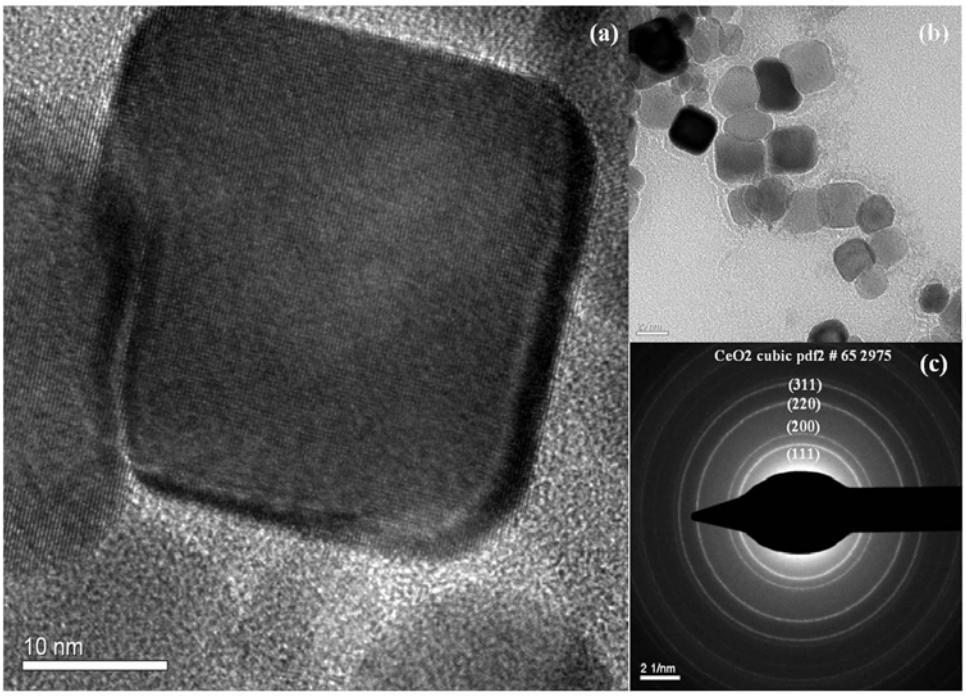

Figure 3.10. (a) HRTEM image of a single CeO_2 nanocube synthesized at 240°C for 24 h. in presence of NaOH. Insets show (b) TEM image of cubic nanoparticles and (c) SAED pattern.

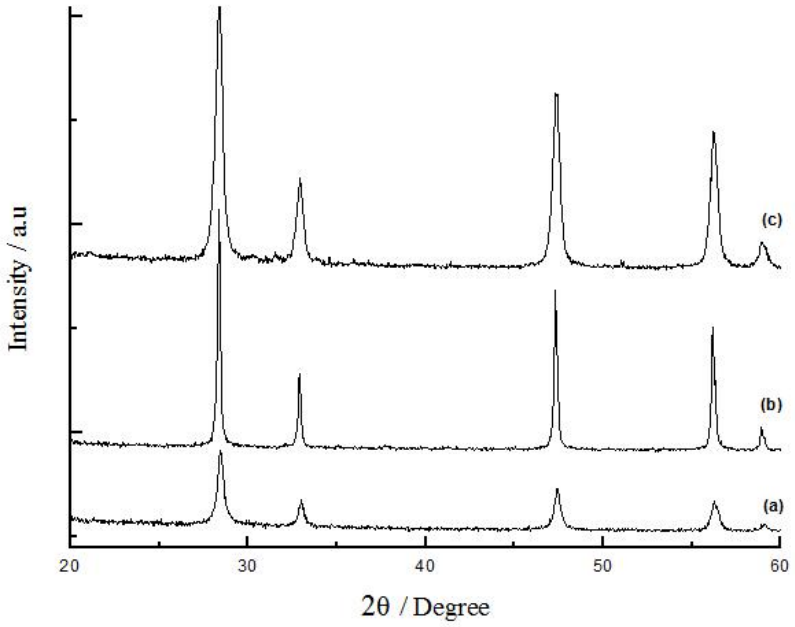

Figure 3.11. XRD patterns of the precipitated powders obtained from aqueous solutions containing CeO_2.The heating temperature was 240°C for 24 h. The used base was (a) KOH, (b) NaOH and (c) LiOH.

Table 3.2. Average crystallite sizes calculated from the most intense (111) XRD peak as a function of alkali base type and concentration

Temperature; 240°C	Starting Bases		
Concentrations (M)	LiOH (nm)	NaOH (nm)	KOH (nm)
0.1	17.67	15.58	14.59
0.5	18.14	16.38	14.96
5	23.60	21.72	20.56
8	55.36	53.79	36.21

According to Table 3.2. average crystallite size of CeO_2 nanoparticles are both concentration and alkali base type dependent. Increasing concentration of alkali base in solution causes to increase average crystallite size. High base concentration is required for the growth of nanoparticles in size. Also, as going down in a 1A group of periodic table results in smaller nanoparticles in size.

Particle size distribution was determined by measuring over 100 particle size from TEM images and shown in Figure 3.12. Average particle sizes were varied with alkali base change. Experiments in presence of 8M LiOH alkali base provided average 40 nm and 8M KOH alkali base provided average 56 nm particle size. Using 8M NaOH alkali base gives bigger nanoparticles with an average particle size of 158 nm. These particle sizes are not consistent with crystallite sizes as they are completely different. Analysis of profile parameters in X-ray patterns is used to determine the crystallite size. When XRD measures the crystallite size, it probably detects the single crystal within the particle. Size analysis with profile widths gives the crystallite size. Domains that are separated by domain walls may exist within the particles. These domains cannot be detected with TEM or SEM. They only detect the particle sizes. Particle size measurement is done to the whole powder after crystal growth and it can contain more than one crystal. Therefore, it is logical to have larger particle size than crystallite size.

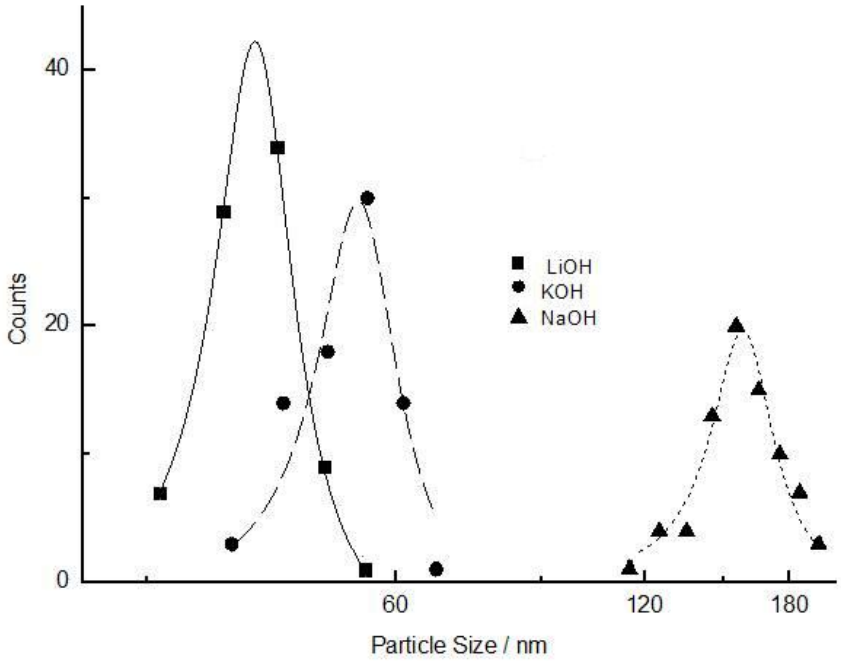

Figure 3.12. Particle size distributions of CeO_2 nanoparticles synthesized with LiOH, NaOH and KOH respectively.

3.2.2. Effect of Reaction Time

In order to fully understand the formation process of CeO_2 nanoparticles, time-dependent experiments were carried out to monitor the evolving process by fixing the temperature of reaction at 240°C. Initially, products were synthesized with 8M NaOH alkali base for the time intervals 1, 2, 4, 8, 16 and 24 h respectively. The series of SEM images in Figure 3.13. show that 24 hours reaction time was the best choice for fabrication CeO_2 nanoparticles. When the reaction time was increased, the morphological transformation of nanoparticles favors from aggregated species to the cubic shape species. With the extension of time, CeO_2 nanoparticles may complete their nucleation and the growth of nanoparticles was based on the Ostwald ripening process that makes the crystallinity improved and the diameter grew. So, the aggragates recrystallize into single-crystalline nanocubes.

After, same experiments were repeated using 8M KOH and 8M LiOH in the fabrication, the morphological evolution of CeO_2 nanoparticles against time was investigated. Similar results were found and the optimum condition was found as 24 h for both alkali bases. Results are shown in Figure 3.14. for LiOH alkali base and Figure 3.15. for KOH alkali base.

Average crystallite sizes were determined from XRD patterns, illustrated in Figure 3.16., by applying FWHM to the most intense peak (111) using Scherrer equation. These crystallite size calculations were done all experiments in presence of these three bases. Results are shown in Table 3.3. below and the reaction time significantly effect the growth of nanoparticles. It enhances the nucleation rate.

Table 3.3. Average crystallite sizes calculated from the most intense (111) XRD peak as a function of reaction time.

Temperature; 240^{o}C	Average Crystallite Size (nm)		
Reaction Time	LiOH	NaOH	KOH
1	22.62	33.83	25.08
2	23.07	34.68	28.26
4	24.45	35.09	31.18
8	26.13	37.68	33.44
16	30.76	43.87	34.78
24	55.36	53.79	36.21

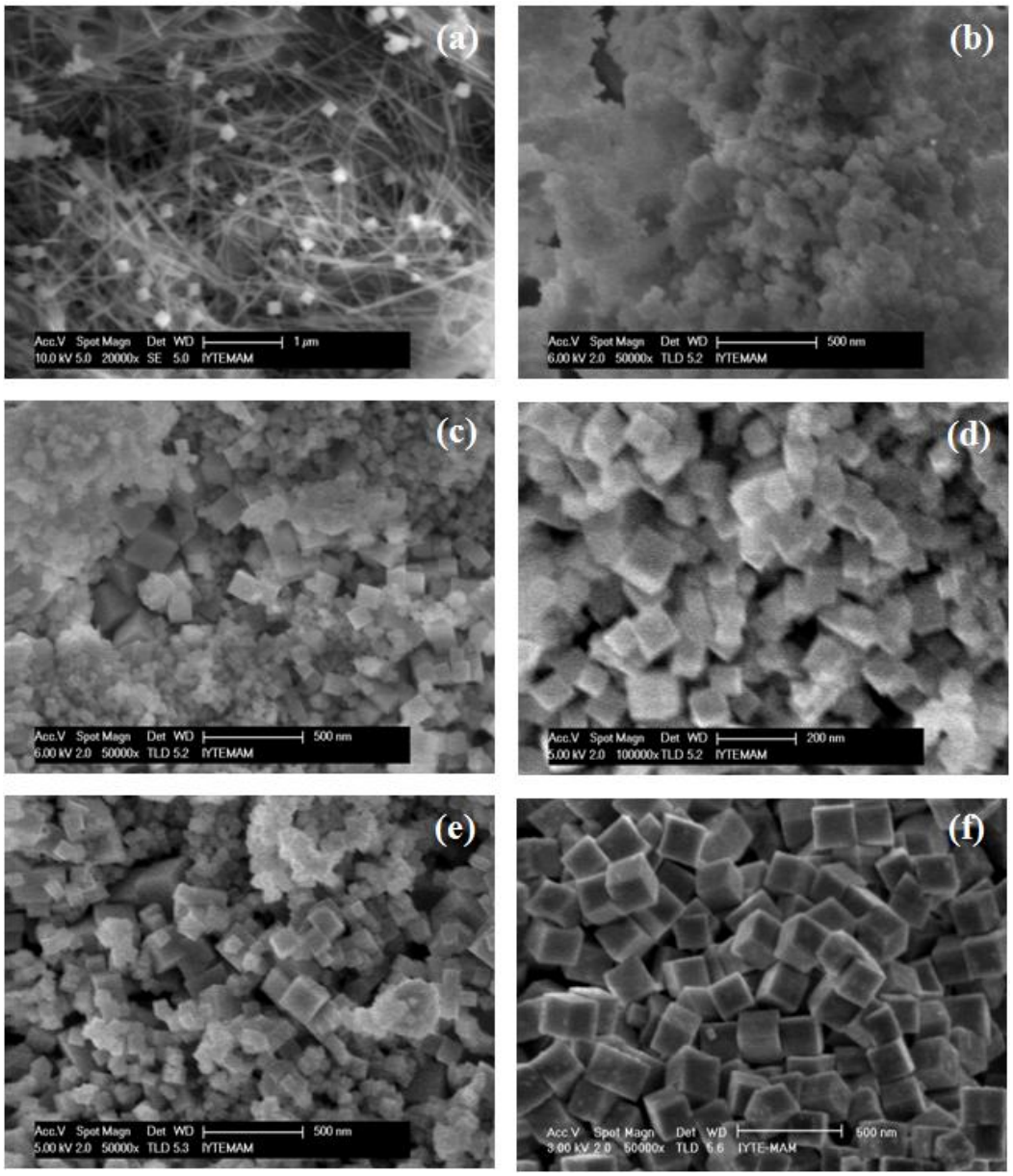

Figure 3.13. Series SEM images of morphology evolution of cubic CeO_2 nanoparticles with the stepwise prolonged reaction time (a) 1 h, (b) 2 h, (c) 4 h, (d) 8 h, (e) 16 h and (f) 24 h. Used base was NaOH.

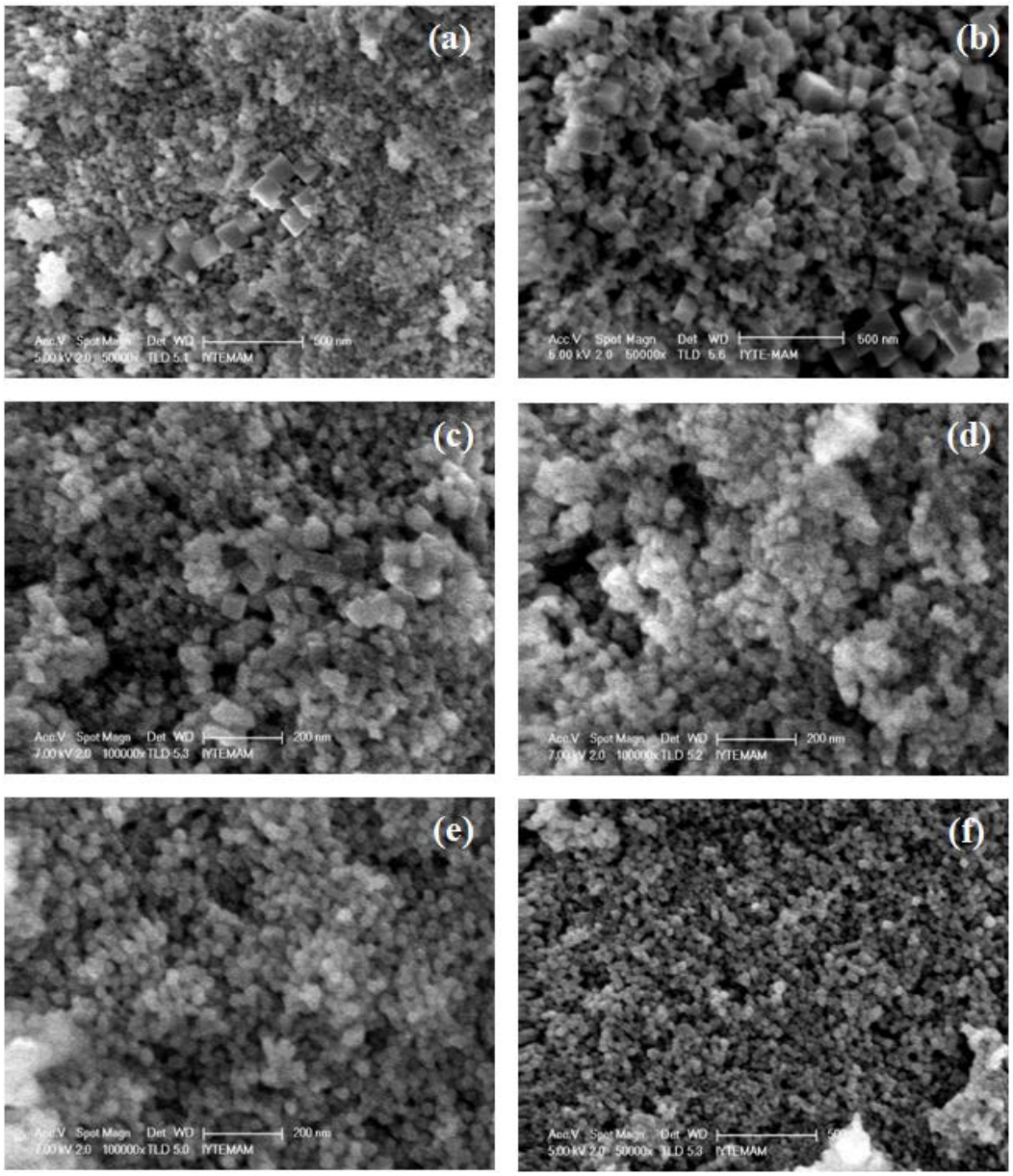

Figure 3.14. Series SEM images of morphology evolution of cubic CeO_2 nanoparticles with the stepwise prolonged reaction time (a) 1 h, (b) 2 h, (c) 4 h, (d) 8 h, (e) 16 h and (f) 24 h. Used base was LiOH.

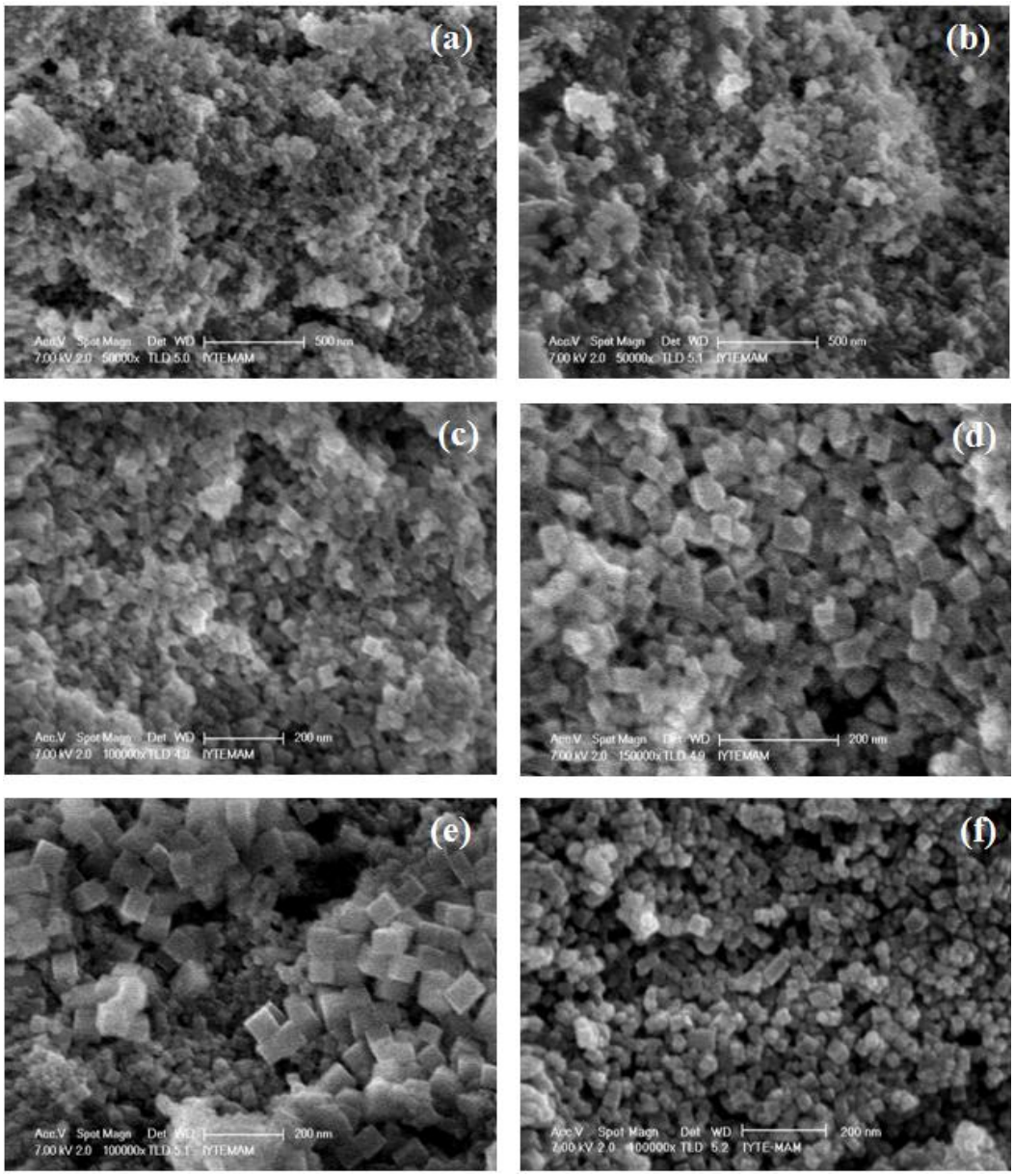

Figure 3.15. Series SEM images of morphology evolution of cubic CeO_2 nanoparticles with the stepwise prolonged reaction time (a) 1 h, (b) 2 h, (c) 4 h, (d) 8 h, (e) 16 h and (f) 24 h. Used base was KOH.

XRD pattern of NaOH alkali base as a function of time are shown in Figure 3.16. Reflections were indexed to pure cubic CeO_2 fluorite structure. Experiments done with LiOH and KOH gave the same result and they are not shown on this study.

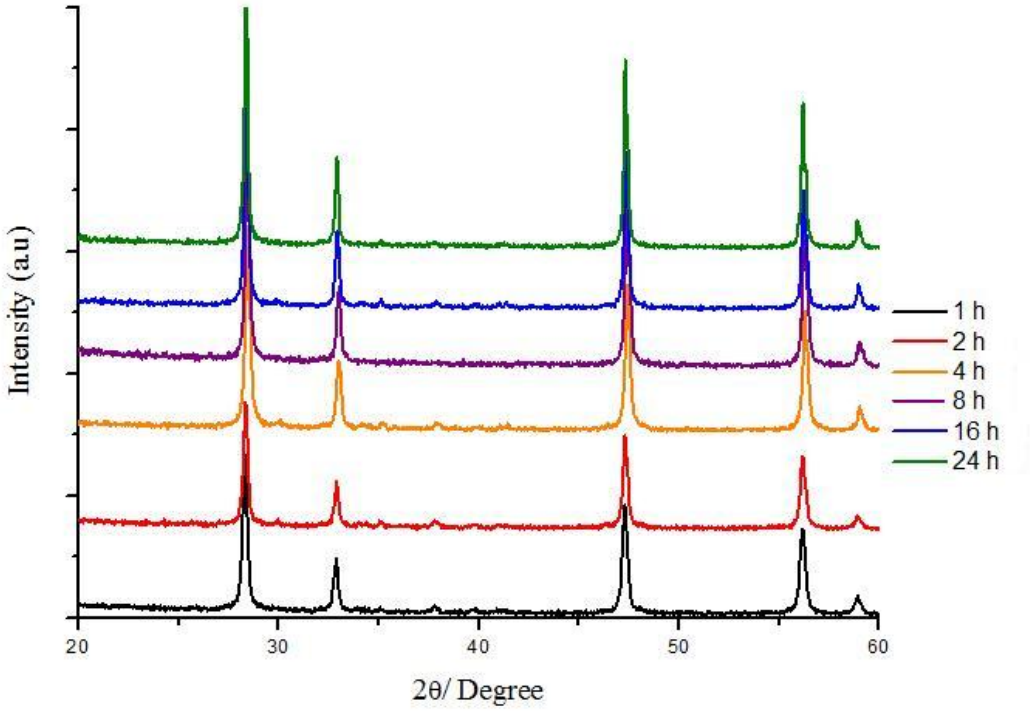

Figure 3.16. XRD pattern of CeO_2 nanoparticles in presence of NaOH for different reaction time intervals.

Furthermore, particle growth kinetics study was done in order to fully understand the evolution of nanoparticles against reaction time. Growth kinetics affects the electronic and mechanical properties of nanomaterials especially doped with other materials. They allow investigating the diffusion mechanisms of both pure ceria and doped ceria. Particle size distributions that are shown in Figure 3.17., Figure 3.18. and Figure 3.19. were determined by measuring over 100 particle sizes from SEM images. When the reaction time was increased, it caused particle sizes to increase. Then, the grain-growth depended on time analysed with the following equation:

$$D^n - D_o^n = Kt \tag{3.1}$$

and

$$K = K_o \exp\left(\frac{-Q}{RT}\right) \tag{3.2}$$

where D^n is the grain size at time, t, D_o^n is the average grain size at time, t=0, n is the grain exponent, K is the rate constant, K_o is the preexponential constant, Q is the activation energy of grain growth, R and T are the gas constant and absolute temperature.. For thermally activated processes ($D>D_o$), these equation can be simplified as;

$$D^n = K_o \exp\left(\frac{-Q}{RT}\right)t \tag{3.3}$$

In a constant temperature range, Q is a constant. Thus, grain exponent (n) can be found from slope of the plot of lnD vs. lnt which is illustrated in Figure 3.20. Particle growth rates were shown on Table 3.4. Based on this, cerium oxide nanoparticles synthesized with LiOH and KOH gave smaller particle growth rates, however, nanoparticles synthesized with NaOH gave rather higher growth rate.

Table 3.4. Particle growth rates of CeO_2 nanoparticles in presence of different alkali bases.

Alkali Base	Particle Growth Rate (n value)
LiOH	3.3
NaOH	4.1
KOH	3.5

Studies on grain growth kinetics found similar results, Chen and Chen (1996) found pure CeO_2 grain growth, obtained with homogeneous precipitation method, as 2, Zhang, et al. (2002) found the grain growth of nanoparticles, prepared by conventional mixed oxide method, as 3. We found somewhat higher than their results. The reason is may be our chemically synthesized materials have higher reactivity (Zhang, et al. 2003).

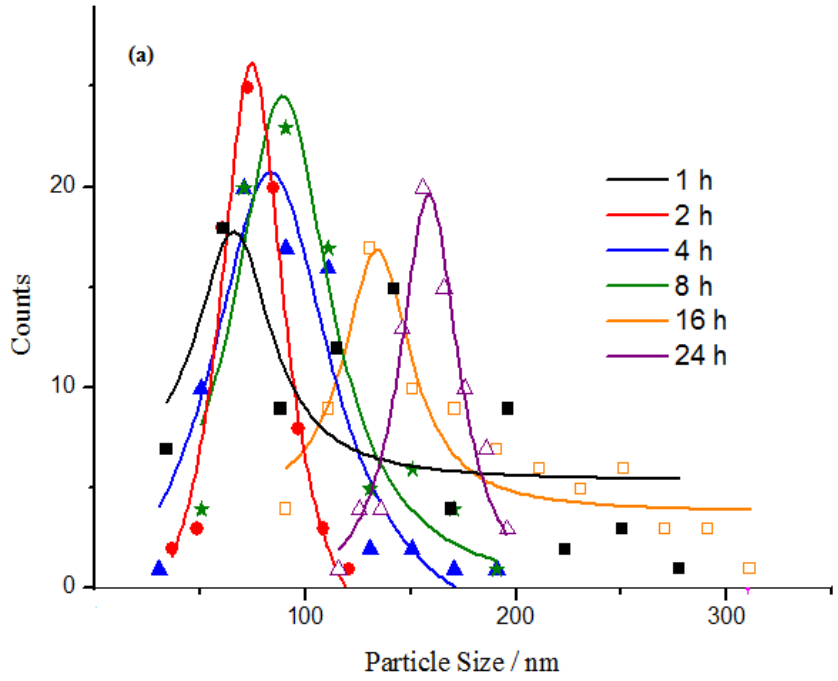

Figure 3.17. Particle size distribution of CeO_2 nanoparticles in presence of NaOH alkali base under different reaction times.

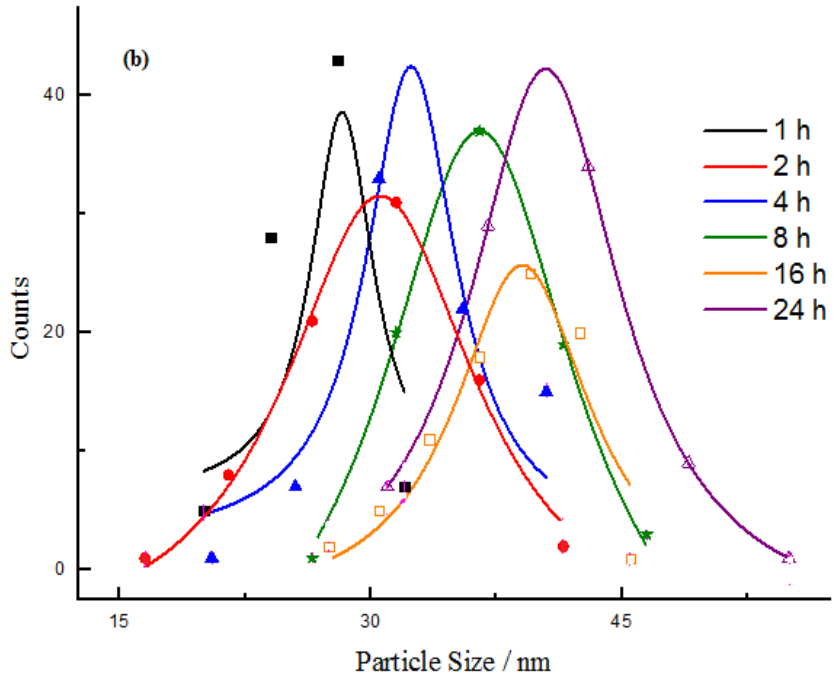

Figure 3.18. Particle size distributions of CeO_2 nanoparticles in presence of LiOH alkali base under different reaction times.

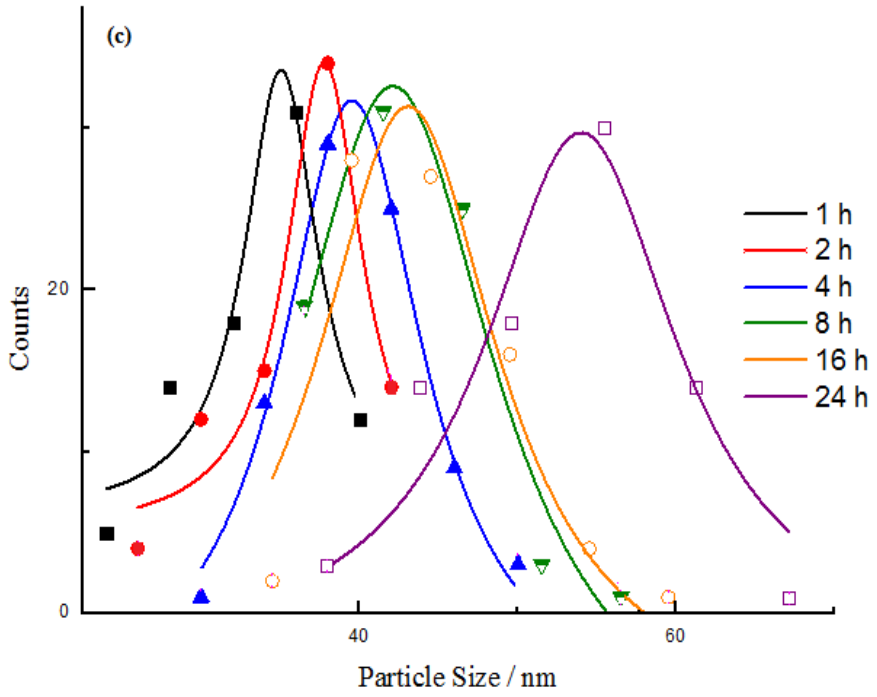

Figure 3.19. Particle size distributions of CeO_2 nanoparticles in presence of KOH alkali base under different reaction times.

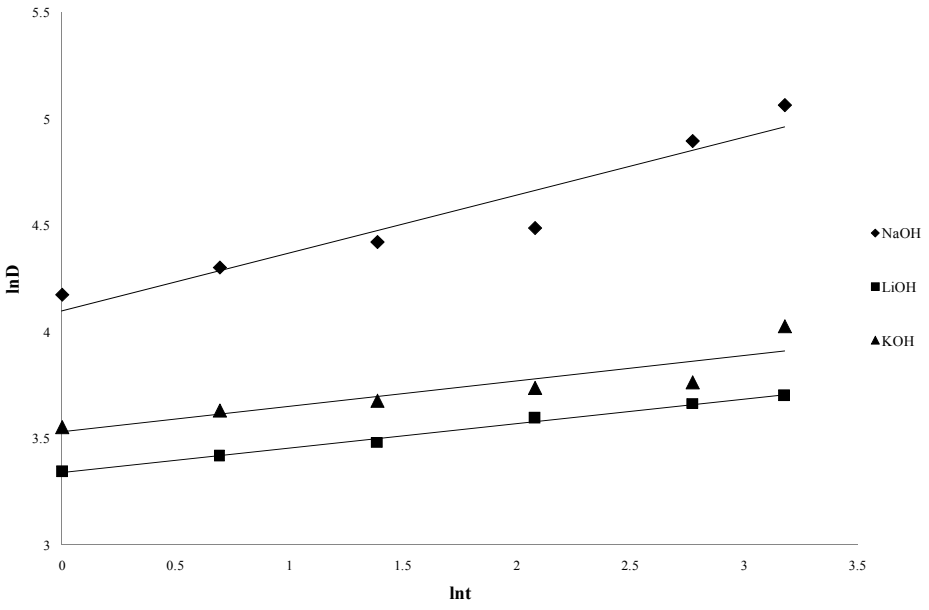

Figure 3.20. Plot of lnD vs. lnt for different alkali bases. The values of n were calculated from the slope of the best fit lines.

3.2.3. Effect of Reaction Temperature

The effect of hydrothermal reaction temperature on particle morphology and crystallite size was determined. We observed rod-shaped nanoparticles at 120°C as reported in literature (Yang et al. 2007). Their results were only contained NaOH alkali base. Thus, we enlarged the study with doing three bases of NaOH, KOH and LiOH. After 120°C, rod-shaped nanoparticles began to transform into cubic shape as temperature accelerates the crystal growth and nucleation of nanoparticles as it is illustrated in Figure 3.21. At 160°C some nanocubes with a lot of aggragation occured. At 200°C nanocubes appeared predominantly and 240°C was the optimum temperature for transforming all particles into cubic shape. Figure 3.22. and Figure 3.23. shows the results in presence of LiOH and KOH alkali bases respectively. X-ray Diffraction studies show that increasing temperature promotes the formation of pure CeO_2 nanoparticles as can be seen in Figure 3.24. in presence of NaOH alkali base.

The precipitated crystalline Ce_2O_3 ceria dissolves in water when the temperature is increased. At nucleation step concentration of ceria monomers increases and they recrystallize into nuclei and transform to various shapes.

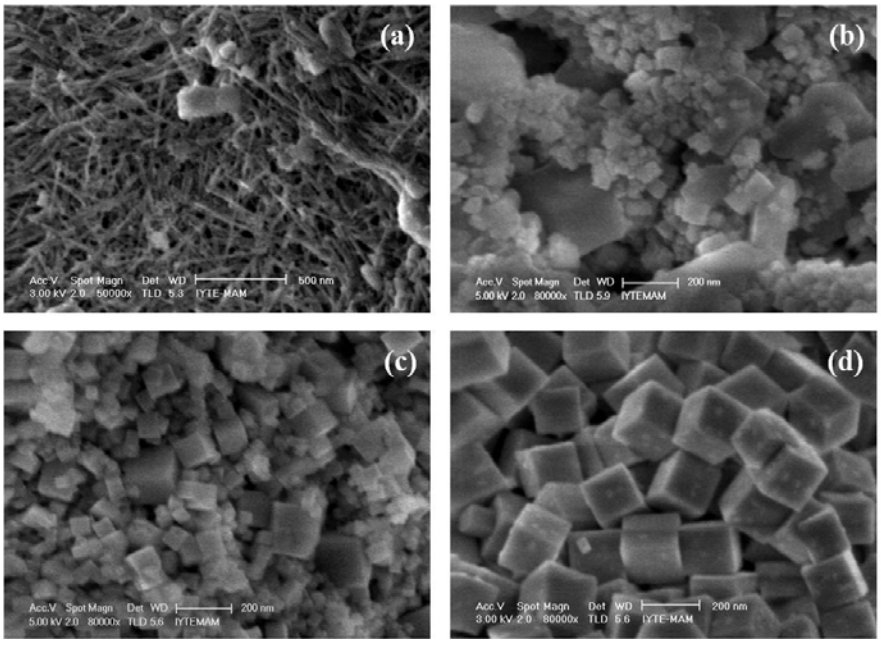

Figure 3.21. SEM images of obtained cubic CeO_2 nanoparticles. The used base was NaOH. and the heating temperature was (a) 120°C, (b) 160°C, (c) 200°C and (d) 240°C for 24 h.

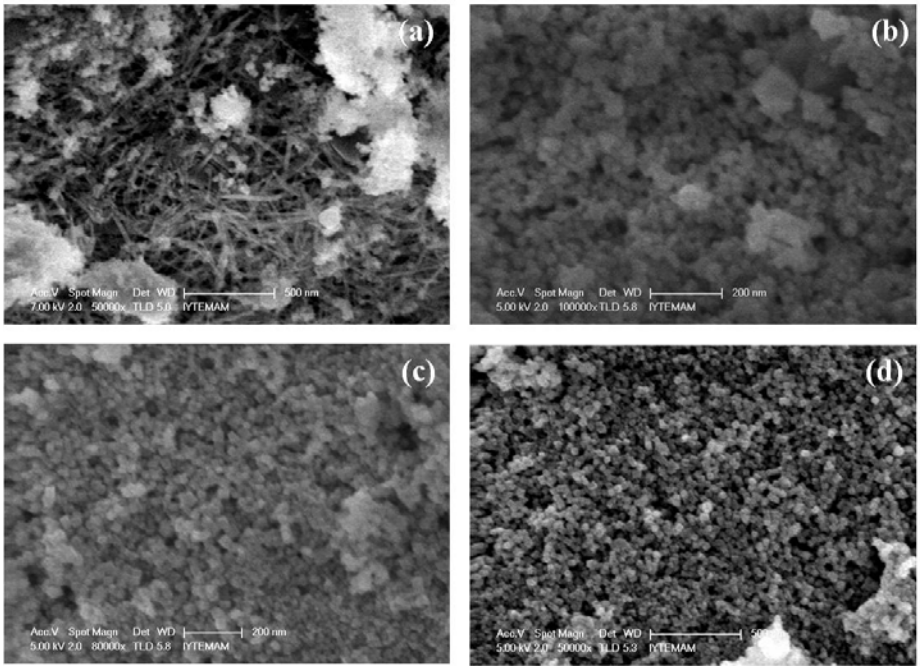

Figure 3.22. SEM images of obtained cubic CeO_2 nanoparticles. The used base was LiOH. and the heating temperature was (a) 120°C, (b) 160°C, (c) 200°C and (d) 240°C for 24 h.

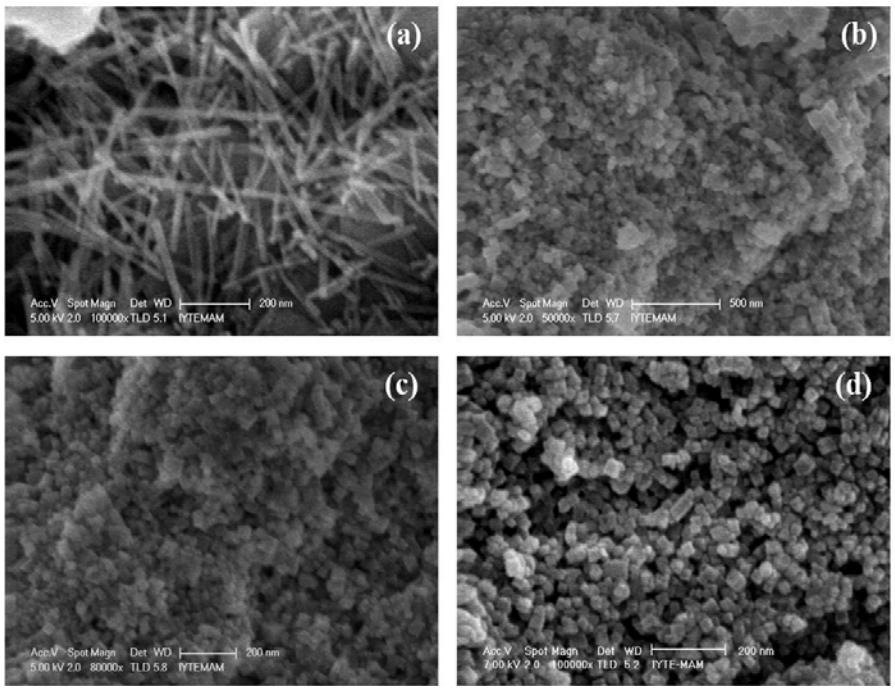

Figure 3.23. SEM images of obtained cubic CeO_2 nanoparticles. The used base was KOH. and the heating temperature was (a) 120°C, (b) 160°C, (c) 200°C and (d) 240°C for 24 h.

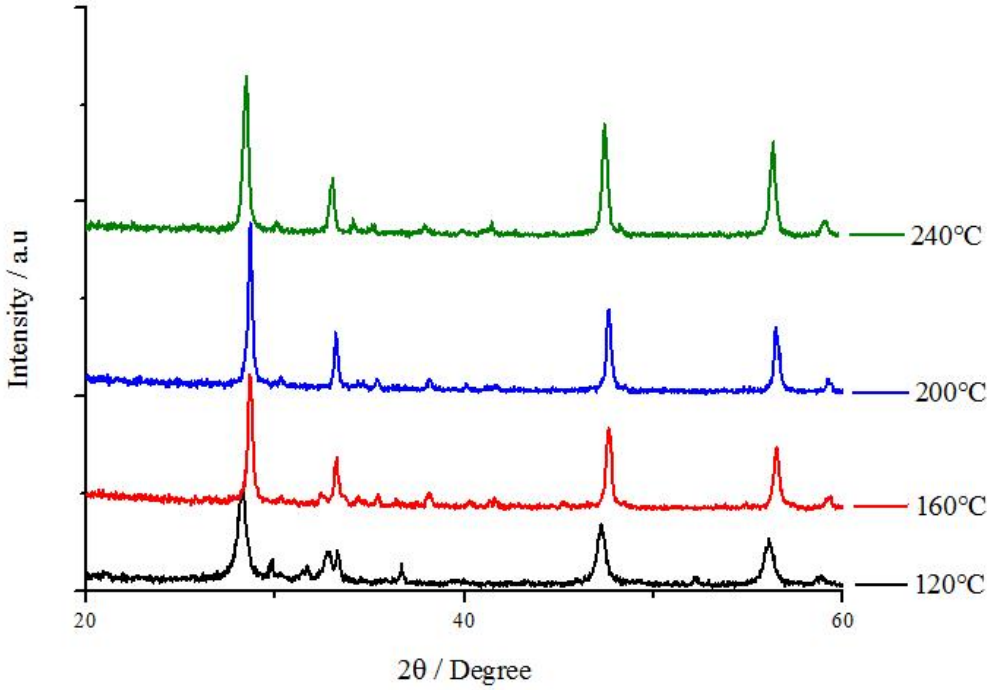

Figure 3.24. XRD patterns of CeO_2 nanoparticles in presence of NaOH under different reaction temperatures.

3.3. Optical Properties of CeO_2 Nanoparticles

The optical properties of semiconductor nanocrystallines have been studied extensively in recent years. Considerable research has been focused on the fluorescence properties of nanomaterials because fluorescence may reveal the presence of crystalline defects resulting from the synthesis process.

All absorbance and fluorometry measurements were done with the particles suspended in deionized water. Because of the low dispersibility of CeO_2 nanoparticles in water, dispersions were ultrasonically agitated for 10 min.

3.3.1. UV-Vis Spectroscopy

Figure 3.25. shows the absorption spectra of CeO_2 nanoparticles synthesized in presence of LiOH, NaOH and KOH. The concentration of dispersions was 1.05 mM and they were synthesized at 240°C for 24 h. A clear absorption edge was observed for each of these bases and the bandgap energy were determined with cutting the wavelength

axis by extrapolating the absorption peak. Measured absorption peaks and bandgaps shown in Table 3.5. Bandgap values are consistent with the literature (Masui, et al. 1997, Yin, et al. 2002).

When moving up the 1A group of periodic table, there is a blue shift in absorbance values of CeO_2 nanoparticles. This result, shows the atomic radius dependence of nanoparticles and also indicates the decreasing particle size. As the particles get smaller, blue shift is observed in the absorbance of material (Deshpande, et al. 2005, Chai, et al. 2001, Tsunekawa, et al. 2000).

Bandgap of CeO_2 nanoparticles in presence of LiOH (3.38eV) is larger than that of bulk (3.2 eV), which is due to the quantum size effect (Yin, et al. 2002). In quantum size region, when the particle size decreases, the bandgap of a semiconductor increases and this results a blue shift in the absorption bands. Based on this phenomenon, LiOH has the lowest particle size that is consistent with our particle size measurements.

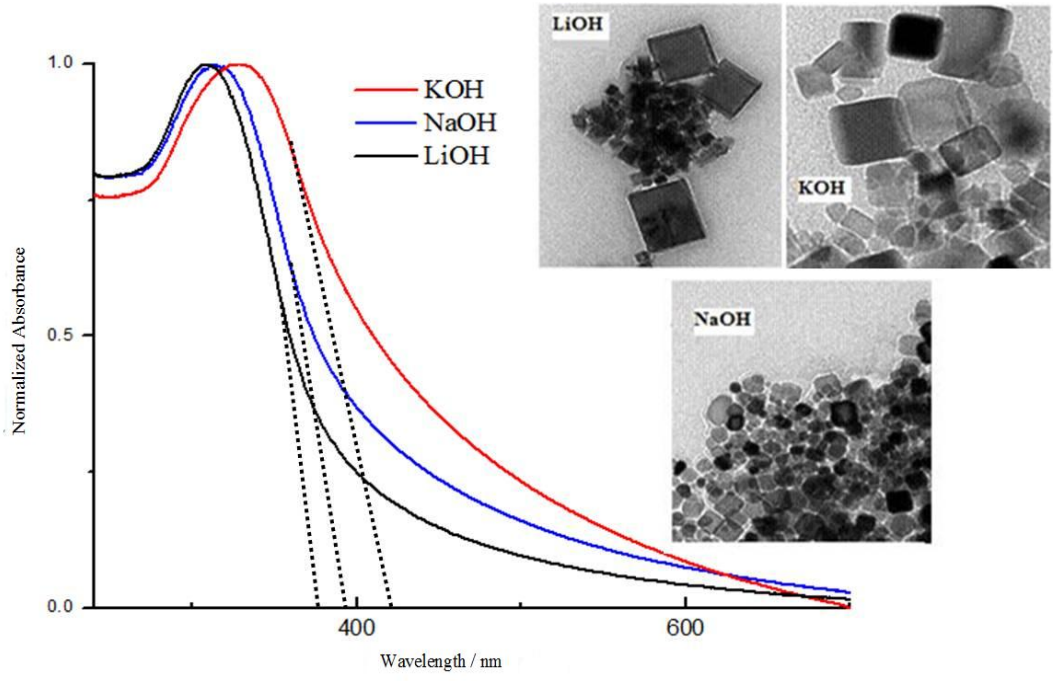

Figure 3.25. UV-Vis Spectra of CeO_2 nanoparticles in presence of LiOH, NaOH and KOH. Insets show the TEM images of nanoparticles.

Table 3.5. Absorption and bandgap energies of CeO_2 nanoparticles

Alkali Base	ONSET (Absorption edge) (nm)	Absorbance (nm)	Bandgap (eV)
LiOH	367	307	3.38
NaOH	392	314	3.17
KOH	415	327	2.98

3.3.2. Fluorescence Spectroscopy

Photoluminescence emission spectra of pure CeO_2 nanoparticles precipitated in the presence of NaOH, LiOH, and KOH at various temperatures, reaction times, and concentrations were recorded for the suspension of the particles in H_2O. The particle suspensions were stable for the time required for the measurements. Additionally, independent measurements of solid-state spectra showed comparable results and confirmed the validity of our experimental method. The emission spectra of the CeO_2 nanoparticles measured at excitation wavelength of 290 nm (4.28 eV), show two emission signals at 400 nm (3.10 eV) and 380 nm (3.27 eV). The second signal can be attributed to the band-edge exciton annihilation, whereas the origin of the first signal is open to debate in literature. One of the common approaches for the possible explanation of this peak was ascribed to the substitutional defect (Ce^{3+}) of cerium oxide in the crystal structure.

Investigations on the temperature dependence of photoluminescence were carried out for further understanding of the optical properties of the prepared CeO_2 nanoparticles. Figure 3.26. presents normalized emission of the particles precipitated from hydrothermal precursor at different temperatures. For all samples, intensities of both emissions increase with temperature. However, relative intensity of the second emission with respect to the emission of excitation annihilation decreases with temperature. This result suggests that emission at 380 nm is the result of a type of impurity Ce(III), which can be considered as substitutional defect.

Ce(III) defect states are considered as hexagonal crystal phase. Increasing temperature favors the face-centered cubic crystal structure to hexagonal crystal structure. Theoretical calculations show that face centered cubic phase is thermodynamically stable. Therefore, the tendency towards the face centered cubic

structure with increasing temperature leads to a decrease in defect sites at higher temperatures (Im and Park 2002).

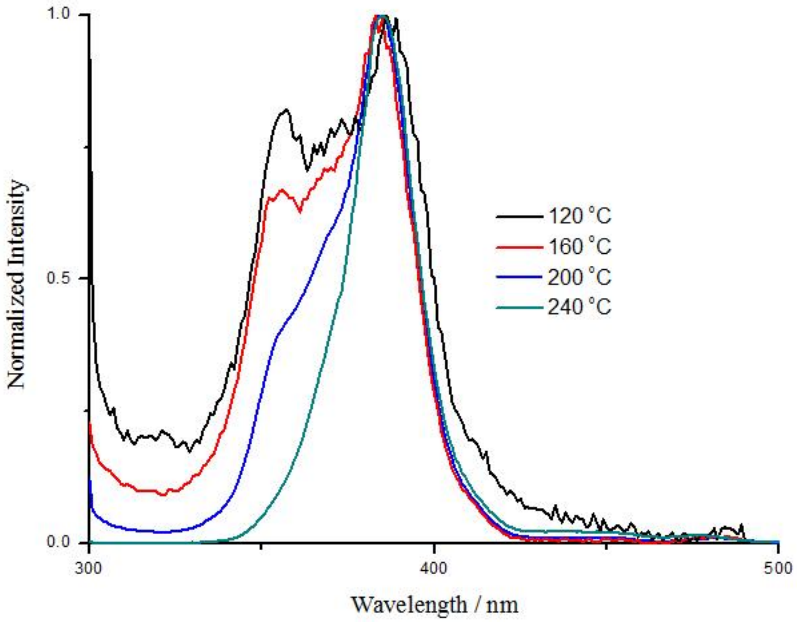

Figure 3.26. Room temperature fluorescescence spectra of the CeO_2 nanoparticle dispersions at different reaction temperatures for 24 h.

Effect of reaction time on fluorescence spectrum of CeO_2 nanoparticles in presence of NaOH was also investigated. In Figure 3.27. defect states of CeO_2 nanoparticles were annealed in a same manner with temperature. Longer reaction times improve nucleation, completeness of crystal growth and allow the particles to find a favorable lattice. Thus, number of defects is reduced.

When alkali effect on fluorescence spectrum is investigated, CeO_2 nanoparticles synthesized in presence of NaOH gives the fluorescence peak containing lowest defect states. As can be seen in Figure 3.28. LiOH and KOH have the defect peak at about 365 nm. This can be related with the particle size distribution results as LiOH and KOH have smaller particles in size and they are blue-shifted.

Alkali concentration effect was determined with NaOH alkali base and concentration dependent defect state was observed. As the concentration was decreased, a small peak located at about 350 nm was appeared like in Figure 3.29. This peak can be attributed to defect state. Also blue shift was observed as the concentration was decreased. A partial dissolution of nanoparticles during dilution could lead to

decreasing size. This blue shift can be explained by charge transitions from 4f band to the valence band of CeO_2 (Yu, et al. 2004).

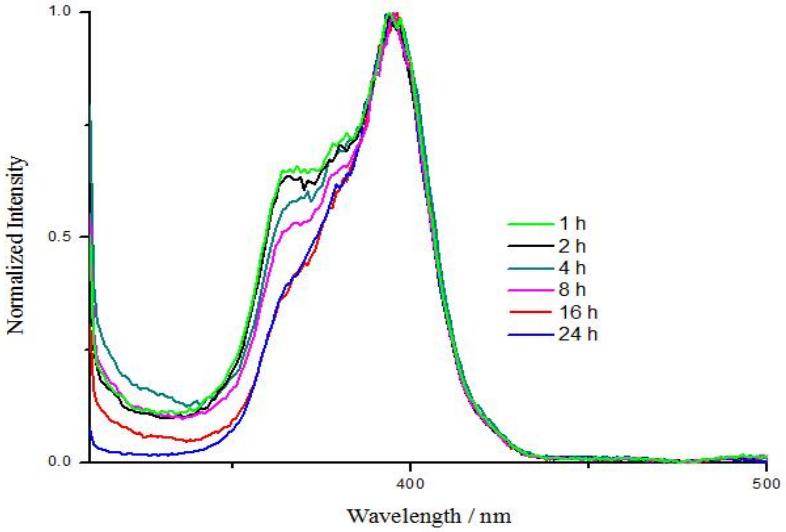

Figure 3.27. Room temperature fluorescecence spectra of the CeO_2 nanoparticle dispersions for different reaction times at 240°C.

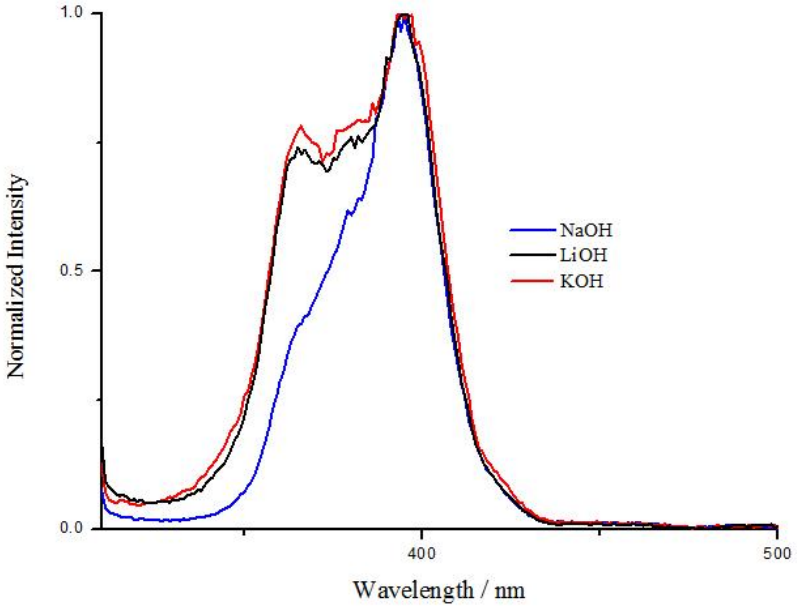

Figure 3.28. Room temperature fluorescence spectra of the CeO_2 nanoparticle dispersions with different alkali bases.

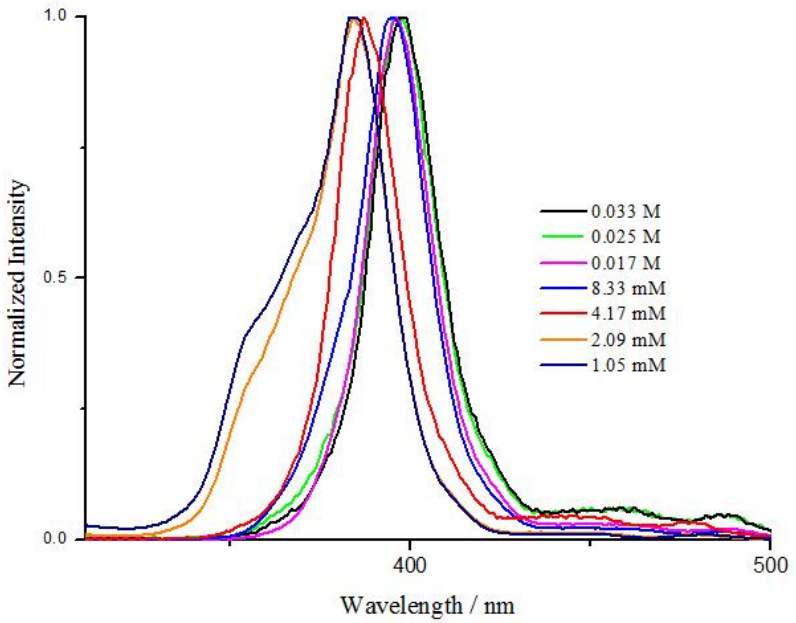

Figure 3.29. Room temperature fluorescence spectra of the CeO_2 nanoparticle dispersions with different concentrations.

3.4. Shape Effect Studies

Various-shaped CeO_2 nanoparticles have synthesized in the literature so far. This diverse shapes and sizes of nanoparticles have extensively affected their chemical and physical properties. Well-shaped nanoparticles show superior properties in industrial fields. Therefore, it is important to synthesize nanoparticles in a controllable manner.

In this study, ceria nanocubes were converted to ceria nanorods by adjusting the temperature. Cubic shapes were formed at high temperatures whereas rod-shaped nanoparticles were revealed at somewhat lower temperatures. Synthesis procedure was the same as discussed before. At 120°C rod-shaped, at 240°C cubic shaped ceria nanoparticles were formed.

Spherical ceria nanoparticles were synthesized using different reaction procedure. We used the procedure of Xu et al. in order to synthesize spherical nanoparticles and compare their properties with other shapes. Typical procedure scheme is illustrated at Figure 3.30. (Xu, et al. 2008).

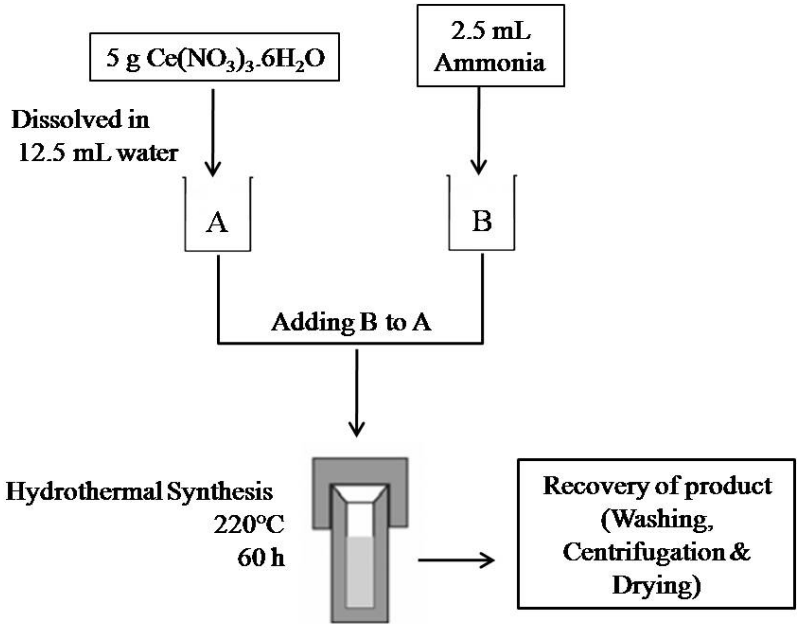

Figure 3.30. Block diagram of the procedure used during the synthesis of sphere CeO_2 nanoparticles

Structural and morphological characterization was done with XRD and SEM techniques. Figure 3.31. shows the corresponding XRD pattern of spherical CeO_2 nanoparticles. XRD pattern of nanorods in Figure 3.24. indicates that the nanoparticles contain hexagonal phase Ce_2O_3 (JCPDS – 78-0484). Figure 3.1. shows the XRD pattern of cubic CeO_2 nanoparticles. Sphere and cubic shaped CeO_2 nanoparticles give pure reflections of CeO_2.

Morphology was evaluated from SEM image of spherical CeO_2 nanoparticles that is illustrated in Figure 3.32. SEM images of rod-shaped and cubic shape CeO_2 are shown on Figure 3.21. It is clear that concentration of existing monomers is a key factor for evolution of the shapes of the resulting nanocrystals. The required monomer concentration in the reaction solution increases from rods to spherical shapes and then more branched structures (Peng 2003). This monomer concentration strongly depends on the temperature and as the temperature is gradually increased, solubility of ceria increases and also chemical potential of the environment increases. Finally, increasing solubility and chemical potential result in nuclei with high energy configuration and morphology. As a recall, we synthesized rod-shaped ceria nanoparticles at 120°C, spherical ceria nanoparticles at 220°C and cubic ones at 240°C.

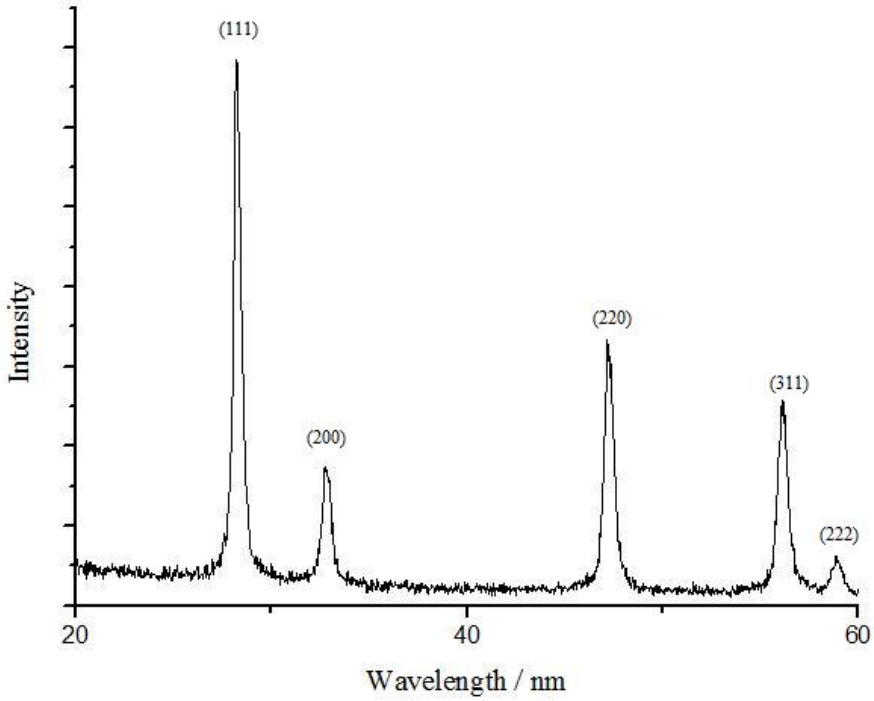

Figure 3.31. X-ray diffraction patterns of the precipitated powders of spherical shaped CeO_2 nanoparticles.

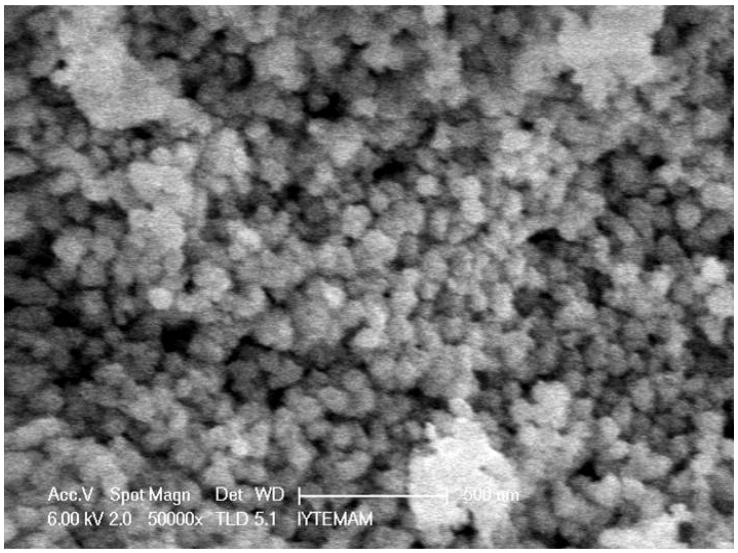

Figure 3.32. SEM image of spherical CeO_2 nanoparticles

Furthermore, effect of shape on optical properties of nanoparticles was investigated. UV-Vis spectra of rod-shaped, spherical and cubic shaped CeO_2 nanoparticles are illustrated in Figure 3.33. Rod-shaped CeO_2 nanoparticles have higher

absorbance than other shapes due to its high cross-section that means high likelihood of interaction between sample and light. Absorption edge and bandgap values are varied in accordance with shapes. All bandgap energies are summarized in Table 3.6.

Table 3.6. Bandgap energies of various shaped CeO_2 nanoparticles

Shape of CeO_2 Nanoparticles	ONSET (Absorption edge) (nm)	Bandgap (eV)
Spherical	370	3.38
Cubic	392	3.17
Rod-shaped	402	3.09

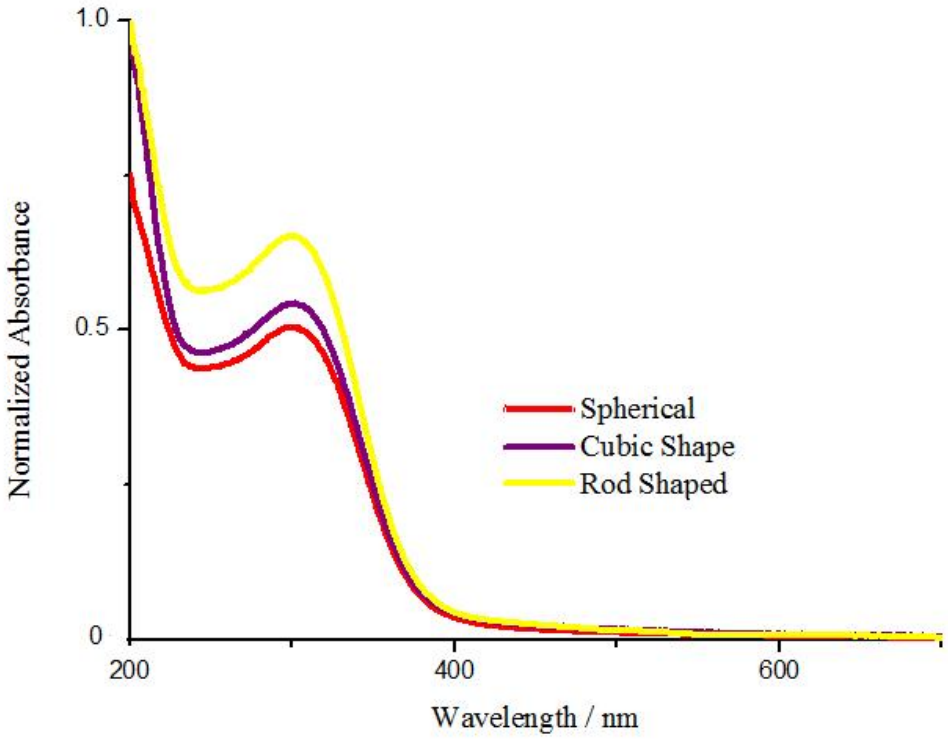

Figure 3.33. UV-Vis spectra of various shaped CeO_2 nanoparticles.

Fluorescence spectra of CeO_2 nanoparticles are shown in Figure 3.34. Both effect of concentration and shape are investigated and again it is found that concentration is an important factor to eliminate defect formation in nanoparticles and this result does not depend on shape. In every different shape CeO_2 nanoparticles, increasing concentration reduces the defect formation. Among the shapes of CeO_2

nanoparticles, spherical shape has more defect than the other shape. While growing stage of nanoparticles, cubic ones grow three dimensional inside and have little defect. Rod-shaped ones have only defects on their edges whereas spherical ones have many defects due to the growing scheme. These growing mechanisms are illustrated as in Figure 3.35.

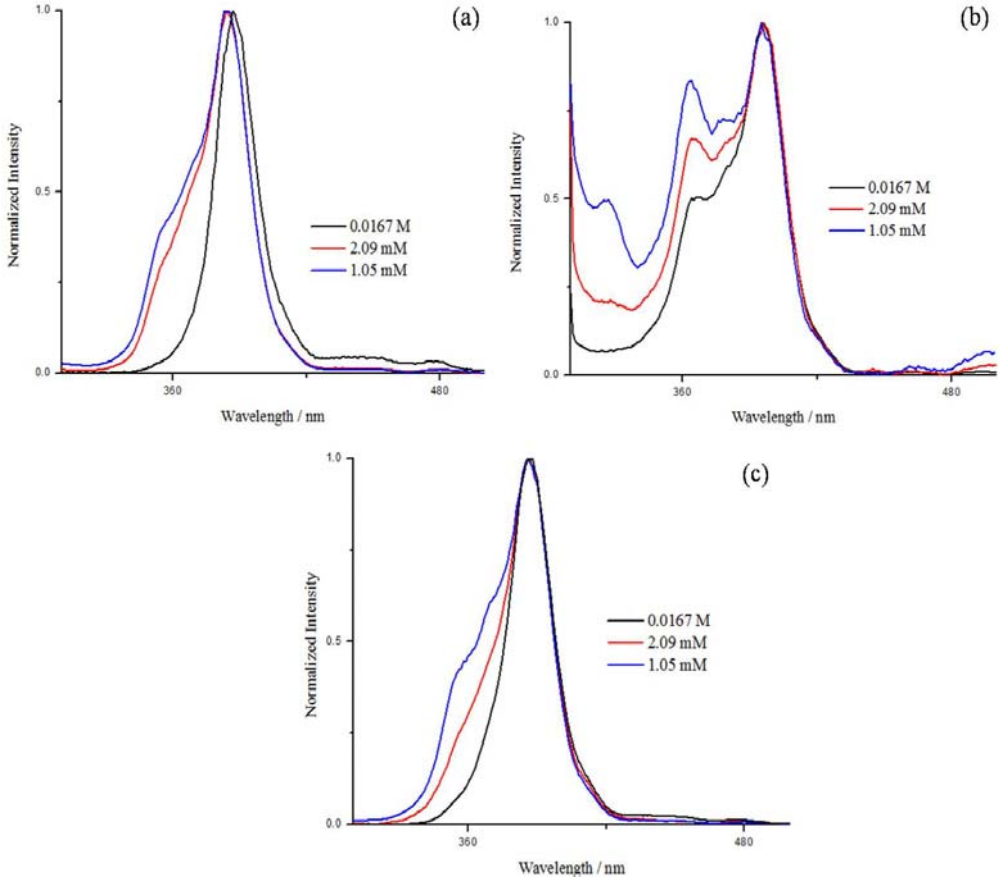

Figure 3.34. Fluorescence spectra of various shape CeO_2 nanoparticles at different concentrations, (a) cubic shape, (b) spherical shape and (c) rod-shape.

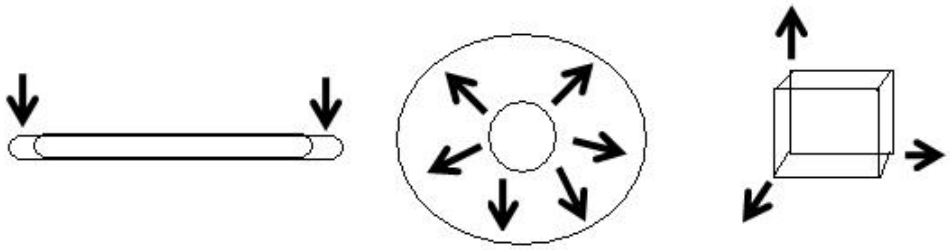

Figure 3.35. Growing mechanisms of rod, spherical and cubic shape CeO_2 nanoparticles

CHAPTER 5

CONCLUSION

Cerium oxide nanoparticles were successfully synthesized via hydrothermal method. As-synthesized particles were characterized using XRD, SEM, TEM and spectroscopic methods. This study was divided into three parts. In the first part of the study, reaction temperature, reaction time, alkali type and alkali concentration on morphology and crystalline nature of CeO_2 nanoparticles were investigated.

Three bases from 1A group of the periodic table were chosen and cubic CeO_2 nanoparticles were synthesized in presence of LiOH, NaOH and KOH. It was found that both alkali type and concentration have strong influence on the formation of nanoparticles. As the concentration of base was increased, size of nanoparticles increased. The average crystallite size of nanoparticles decreased with both decreasing concentration and increasing atomic radius of alkali bases.

Reaction time studies were performed in order to fully understand the formation process of CeO_2 nanoparticles. Morphology evolution of nanoparticles was done with the stepwise prolonged reaction time of 1, 2, 4, 8, 16 and 24 h. It was found that 24 h is the optimum time for obtaining single crystalline CeO_2 nanoparticles. Shorter reaction times gave aggregated nanoparticles and increasing reaction time allowed to grow larger nanoparticles based on the Ostwald ripening process.

Grain growth kinetics study was done to monitor the structural formation against reaction time. Based on the results, nanoparticles in the presence of NaOH grew much faster than the other bases.

Furthermore, reaction temperature also strongly affected the morphology. Increasing temperature caused precipitated amorphous ceria to dissolve in water and at the nucleation step, concentration of ceria monomers increased and recrystallized into nuclei to form desired shape.

The second part of this study was to investigate optical properties of synthesized CeO_2 nanoparticles. Based on the UV-Vis spectroscopy measurements, a clear absorption band was observed for all three bases. Moving upwards on the 1A group of periodic table, absorption peaks were blue-shifted. This result indicated atomic radius

dependence of nanoparticles and also decreasing Ce(III) defect states with decreasing particle size. LiOH was more blue-shifted and smaller in particle size, whereas KOH was more red-shifted, more defective and had higher formation rates. Also, band gap energies were calculated from UV-Vis spectra and LiOH had the highest bandgap due to its smaller size.

Controlling effects again studied with fluorescence spectroscopy, reaction temperature and reaction time affected CeO_2 nanoparticles in the same manner. Defect formation can be determined from fluorescence spectrum and increasing reaction time of reaction temperature caused to decrease defect formation in nanoparticles. When the alkali concentration was decreased, defect formation was observed while peaks were blue-shifted. When the alkali base type was changed, the results showed less defective CeO_2 nanoparticles can be obtained by using NaOH alkali base.

The last part of the study was to study shape effects on both morphology and optical properties of CeO_2 nanoparticles. Spherical shape nanoparticles were obtained via different procedure. The main result is the conversion of rod-shaped nanoparticles to cubic shape ones by adjusting the temperature. It was found that the key factor was the ceria monomer concentration. High temperature increased solubility of monomers and increasing solubility resulted in high energy configuration and morphology.

Shapes directly affected the optical properties of nanoparticles. Rod-shaped CeO_2 nanoparticles had higher absorbance than spherical and cubic ones due to the high cross-section. Based on fluorescence spectroscopy measurements, spherical shape nanoparticles had more defect than the others.

REFERENCES

Barrer, R.M. 1948. Syntheses and reactions of mordenite. *Journal of Chemical Society*. 2158.

Byrappa, Kullaiah, and Masahiro Yoshimura, eds. 2001. *Handbook of Hydrothermal Technology, A technology for Crystal Growth and Material Processing*. Noyes, New Jersey.

Byrappa, K. and Adschiri, T. 2007. Hydrothermal technology for nanotechnology. *Progress in Crystal Growth and Characterization of Materials*. 53:117-166.

Campbell, C.T. and Peden, C.H.F. 2005. Oxygen vacancies and catalysis on ceria surfaces. *Science*. 309:713-714.

Cao, Guohong. 2004. *Nanostructures and Nanomaterials*. Singapore: World Scientific Publishing Company.

Capek, Ignac. 2006. *Nanocomposite Structures and Dispersions*. The Netherlands: Elsevier B.V.

Carnes, C.L., Kapoor, P.N. and Klabunde, K.J. 2002. Synthesis, characterization and adsorption studies of nanocrystalline aluminum oxide and a bimetallic nanocrystalline aluminum oxide/magnesium oxide. *Chemistry of Materials*. 14: 2922-2929.

Chai, C., Yang, S., Liu, Z., Liao, M., Chen, N., Wang, Z. 2005. The PL "violet shift" of cerium dioxide on silicon. *Chinese Science Bulletin*. 46:2046-2048(24).

Chen, P.L. and Chen, I.W. 1993. Reactive Cerium(IV) oxide powders by the homogeneous precipitation method. *Journal of American Ceramic Society*. 76:1577-1583(6).

Chen, P.L. and Chen, I.W. 1996. Grain growth in CeO_2 : Dopant effects, defect mechanism and solute drag. *Journal of American Ceramic Society*. 79:1793-1800.

Cullity, B.D. 1978. *Elements of X-ray Diffraction*. Massachusetts: Addison-Wesley Publishing Company.

Deshpande, S., Patil, S., Satyanarayana, K., Seal, S. 2005. Size dependency variation in lattice paramater and valency states in nanocrystalline cerium oxide. *Applied Physics Letters*. 87:133113(3pp).

Goodhew, Peter J., John Humphreys, and Richard Beanland, eds. 2001. *Electron Microscopy and Analysis*. New York: Taylor and Francis.

Goranson, R.W. 1931. Solubility of water in granite magmas. *American Journal of Science*. 22:481-502.

Habashi, F. 1994. Recent advances in pressure leaching technology. *First Intl. Conf. Solvothermal Reactions*. 13-16.

Hannink, Richard and June Hill. 2006. *Nanostructure Control of Materials*. Woodhead Publishing in Materials.

Holister, Paul. 2002. Nanotech The Tiny Revolution. *CMP Cientifica*. http://www.nanotech-now.com (accessed April 4, 2009).

Im, S.H. and Park, O.O. 2002. Effect of evaporation temperature on the quality of colloidal crystals at the water-air interface. *Langmuir*. 18:9642-9646(25).

Imanaka, N., Masui, M., Hirai, H., Adachi, G. 2003. Amorphous cerium-titanium solid solution phosphate as a novel family of band gap tunable sunscreen materials. *Chemistry of Materials*. 15:2289-2291(12).

Integrated Laboratory Systems, Incorporated. 2006. *Chemical Information Profile for Ceric Oxide*. Research Triangle Park, NC

Kang, Suk-Joong L. 2005. *Sintering – Densification, Grain Growth & Microstructure*. Butterworth-Heinemann.

Kaya, C., He, J.Y., Gu, X., Butler, E.G. 2002. Nanostructured ceramic powders by hydrothermal synthesis and their applications. *Microporous and Mesoporous Materials*. 54:37-49.

Khodadadi, A., Mohajerzadeh, S.S., Mortazavi, Y., Miri, A.M. 2001. Cerium oxide/SnO_2 based semiconductor gas sensors with improved sensitivity to CO. *Sensors and Actuators B*. 80:267-271.

Komarneri, S. 2003. Nanophase materials by hydrothermal, microwave-hydrothermal and microwave-solvothermal methods. *Special Section: Nanoscience and Nanotechnology*. 85:1730-1734(12).

Kosynkin, V.D., Arzgatkina, A.A., Ivanov, E.N., Chtoutsa, M.G., Grabko, A.I., Kardapolov, A.V., Sysina, N.A. 2000. The study of process production of polishing powder based on cerium dioxide. *Journal of Alloys and Compounds*. 303:421-425.

Laudise, Robert A. 1970. *The Growth of Single Crystals*. Prentice Hall: Englewood Cliffs, NJ.

Lian, H., Zhang, M., Liu, J., Ye, Z., Yan, J., Shi, C. 2004. Synthesis and spectral properties of lutetium-doped CeF_3 nanoparticles. *Chemical Physics Letters*. 395:362-365.

Mai, H., Sun, L., Zhang, Y., Si, R., Feng, W., Zhang, H., Liu, H., Yan, C. 2005. Shape selective synthesis and oxygen storage behavior of ceria nanopolyhedra, nanorods and nanocubes. *Journal of Physical Chemistry B*. 109:24380-24385.

Masui, T., Fujiwara, K., Machida, K., Adachi, G. 1997. Charaterization of cerium(IV) oxide ultrafine particles prepared using reversed micelles. *Chemistry of Materials*. 9:2197-2204.

Miessler, Gary L. and Donald A. Tarr, eds. 2003. *Inorganic Chemistry*. Northfield, Minnesota: Prentice Hall.

Morshed, A.H., Moussa, A.E., Bedair, S.M., Leonard, R., Liu, S.X., El-Masry, N. 1997. Violet/blue emission from epitaxial cerium oxide films on silicon substrates. *Applied Physics Letters*. 70:1647-1649(13).

Nacken, R. 1946. Artificial quartz crystals. *U.S. Office of Technical Services Report*. 18-28.

National Nanotechnology Initiative. 2000. Leading to the Next Industrial Revolution. http://www.nano.gov (accessed April 4, 2009).

Nützenadel, C., Ziittel, A., Chartouni, D., Schmid, G., Schlapbach, L. 2000. Critical size and surface effect of the hydrogen interaction of palladium clusters. *The Europian Physical Journal D.* 8:245-250.

Paul, B.K. and Moulik, S.P. 2001. Uses and applications of microemulsions. *Soft Condensed Matters*. 80:990-1001.

Pavia, Donald R., Gary M. Lampman, and George S. Kriz, eds. 2001. *Introduction to Spectroscopy*

Peng, X. 2003. Mechanisms for the shape-control and shape-evolution of colloidal semiconductor nanocrystals. *Advanced Materials*. 15:459-463(5).

Primet, M. and Garbowski, E. 2002. Fundamentals and applications of ceria in combustion reactions. *Cataytic Science Series, Netherland Institute of Cataytic Research*.

Rabenau, A. 1985. The role of hydrothermal synthesis in preparative chemistry. *Angew Chem (English Ed.)*. 24:1026-1040.

Roy, R. 1994. Acceleration the kinetics of low-temperature inorganic syntheses. *Journal of Solid State Chemistry*. 111:11-17.

Sathyamurthy, S., Leonard, K.J., Dabestani, R.T., Paranthaman, M.P. 2005. Reverse micellar synthesis of cerium oxide nanoparticles. *Nanotechnology*. 16:1960-1964.

Schubert, Ulrich. and Nicola Hüsing, eds. 2000. *Synthesis of Inorganic Materials*. Weinheim, Germany: Wiley-WCH.

Smart, Lesley and Elaine A. Moore, eds. 1996. *Solid State Chemistry – An Introduction*. Cheltenham: Stanley Thornes.

Stambouli, A.B. and Traversa, E. 2002. Solid oxide fuel cells: A review of an environmentally clean and efficient source of energy. *Renewable and Sustainable Energy Reviews*. 6:433-455.

Suda, A., Yamamura, K., Morikawa, A., Nagai, Y., Sobukawa, H., Ukyo, Y., Shinjo, H. 2008. Atmospheric pressure solvothermal synthesis of ceria-zirconia solid solutions and their large oxygen storage capacity. *Journal of Materials Science*. 43:2258-2262.

The Royal Society & The Royal Academy of Engineering. 2004. Nanoscience and Nanotechnologies. http://www.nanotec.org.uk/report/chapter2.pdf (accessed March 28, 2009).

Trovarelli, Alessandro. 2002. *Catalysis by Ceria and Related Materials*. London: Imperial College Press.

Trovarelli, A., Leitenburg, C., Boaro, M., Dolcetti, G. 1999. The utilization of ceria in industrial catalysis. *Catalysis Today*. 353-367.

Tsunekawa, S., Ishikawa, K., Li, Z.Q., Kawazoe, Y., Kasuya, A. 2000. Origin of anomalous lattice expansion in oxide nanoparticles. *Physical Review Letters*. 85:3440-3443(16).

Tsunekawa, S., Fukuda, T. and Kasuya, A. 2000. Blue shift in ultraviolet absorption spectra of monodisperse CeO_{2-x} nanoparticles. *Journal of Applied Physics*. 87:1318-1321(3).

Wang, H., Zhu, J.J., Zhu, J.M., Liao, X.H., Xu, S., Ding, T., Chen, H.Y. 2002. Preparation of nanocrystalline ceria nanoparticles by sonochemical and microwave assisted heating methods. *Physical Chemistry Chemical Physics*. 4:3794-3799.

Wu, G.S., Xie, T., Yuan, X.Y., Cheng, B.C., Zhang, L.D. 2004. An improved solgel template synthetic route to large scale CeO_2 nanowires. *Materials Research Bulletin*. 39:1023-1028.

Xu, J., Li, L. and Li, G. 2008. A facile approach to well-dispersible CeO_2 nanoparticles. *Journal of Dispersion Science and Technology*. 29:1072-1076.

Yan, Z.G. and Yan, C.H. 2008. Controlled synthesis of rare earth nanostructures. *Journal of Materials Chemistry*. 18:5046-5059.

Yang, Z., Zhou, K., Liu, X., Tian, Q., Lu, D., Yang, S. 2007. Single-crystalline ceria nanocubes: Size controlled synthesis, characterization and redox property. *Nanotechnology*. 18:185606(4pp).

Yang, Z., Woo, T.K., Baudin, M., Hermansson, K. 2004. Atomic and electronic structure of unreduced and reduced CeO_2 surfaces: A first-principles study.*Journal of Chemical Physics*. 120:7741-7749(16).

Yin, L., Wang, Y., Pang, G., Koltypin, Y., Gedanken, A. 2002. Sonochemical synthesis of cerium oxide nanoparticles-Effect of additives and quantum size effect. *Journal of Colloid and Interface Science*. 246:78-84.

Yu, S.H., Cölfen, H. and Fischer, A. 2004. High quality CeO_2 nanocrystals stabilized by a double hydrophilic block copolymer. *Colloids and Surfaces A*. 243:49-52.

Zhang, T., Hing, P., Huang, H., Kilner, J. 2002. Sintering study on commercial CeO_2 powder with small amount of MnO_2 doping. *Materials Letters*. 57:507-512.

Zhang, T.S., Ma, J., Kong, L.B., Zeng, Z.Q., Hing, P., Kilner, J.A. 2003. Final-stage sintering behavior of Fe-doped CeO_2. *Materials Science and Engineering B*. 103:177-183.

Zhou, X.D., Huebner, W. and Anderson, H.U. 2002. Room temperature homogeneous nucleation synthesis and thermal stability of nanometer single crystal CeO_2. *Applied Physics Letters*. 80:3814-3816(20).